

**Hydroclimate Data for the Prairies
An Analysis of Possibilities**

**Elaine Barrow (PhD)
May 2010**

Table of Contents

Summary	3
Introduction	4
Data Sources	4
Moisture deficits	9
1. <i>Thornthwaite method</i>	10
2. <i>Simplified Penman-Monteith method</i>	10
A more in-depth look at hydroclimate –an analysis at stream gauge locations	25
Probabilistic Scenarios – where do we go from here?	31
Recommendations	33
Acknowledgements	33
References	33

Summary

This report describes the analysis of a small ensemble of regional climate model (RCM) output over western Canada. Of four available RCM experiments, three were driven by the same GCM, i.e., CGCM3 T47. Examination of the simulated climate normal fields for 1971-2000 showed that the precipitation fields in particular were more realistic when compared to a gridded observed data set than those of the driving GCM. Potential evapotranspiration was calculated using two different methodologies, and moisture deficits (P-PET) for the water year (October – September) and for three summer months (May-June-July) were also calculated. With the exception of RCM3, the RCMs simulated 30-year averages for these hydroclimate variables reasonably well.

Time series for these variables were examined at a number of stream gauge locations in Alberta and Saskatchewan. PET is projected to increase over time in all simulations, as would be expected given the projected increases in temperature. Annual and summer moisture deficits are generally projected to become more severe, although this is site-dependent.

Finally, the prospects for constructing probabilistic scenarios for hydroclimate variables are discussed and recommendations given. Viewing scenarios in a probabilistic manner will allow impacts to be communicated in terms of risk rather than as isolated examples of possible impacts.

Introduction

The aim of this work was to examine available hydroclimate data from both global and regional climate models with a view to developing probabilistic scenarios of prairie drought. In contrast to the many experiments undertaken with global climate models (GCMs) which are readily available, it is only recently that multiple experiments from regional climate models (RCMs) have become available for western Canada. This report examines some results from these RCM experiments and discusses how they may be used in conjunction with GCM output to construct probabilistic scenarios.

Data Sources

Regional climate model (RCM) data were obtained from the North American Regional Climate Change Assessment Program (NARCCAP¹) and the Canadian Centre for Climate Modelling and Analysis (CCCma²). NARCCAP is an international program to produce high resolution climate change simulations in order to investigate uncertainties in regional scale projections of future climate and to generate climate change scenarios for use in impacts research in the United States, Canada and northern Mexico.

For the NARCCAP program, a set of six RCMs was driven by between one and four atmosphere-ocean global climate models (AOGCMs) over a domain covering the conterminous United States and most of Canada (see Table 1). These AOGCMs were forced with the SRES A2 emissions scenario for the 21st century and simulations were also undertaken for the baseline (historical) period. In addition, the RCMs were driven with the NCEP Reanalysis II data for the period 1979-2004. The RCMs were nested within the AOGCMs for the baseline period 1971-2000 and the future period 2041-2070. While data for the Canadian RCM were available through NARCCAP for these two time periods, a longer time series (1960-2100) was obtained directly from the CCCma web site. Of the twelve planned experiments, results from only five are currently available and time constraints meant that only three have been examined in this report. These are described in Table 2. Two of the RCMs selected (CRCM and RCM3) were driven by the latest version of the Canadian coupled GCM - CGCM3 T47 (Flato and Boer, 2001). For the other RCM, HRM3, a custom run of HadCM3 was done specifically for NARCCAP, and this GCM run is not publicly available. The resolution of the RCMs is between 45 and 50 km.

Table 1: Regional – Global Climate Model Combinations available from NARCCAP. Check marks indicate experiments that are currently available (green) or planned and not yet available (red).

Driving GCM \ RCM	GFDL	CGCM3	HadCM3	CCSM	NCEP
CRCM		✓		✓	✓
ECPC	✓		✓		✓
HRM3	✓		✓		✓
MM5I			✓	✓	✓
RCM3	✓	✓			✓
WRFP		✓		✓	✓

¹ www.narccap.ucar.edu

² www.ec.gc.ca/ccmac-cccma/default.asp?lang=En

RCM		Driving GCM	Variables Available*	Time series length
Canadian Climate Model (CRCM)	Regional Model	CGCM3 T47, run 4; Flato and Boer (2001)	T, T _{max} , T _{min} , P	12/1960 – 11/2100
Regional Climate Model version 3 (RCM3)**		CGCM3, run 4; Flato and Boer (2001)	T, P	12/1970 – 11/2000 12/2040 – 11/2070
			T _{max} , T _{min}	12/1970 – 12/1995 11/2040 – 12/2065
Hadley Regional Model 3 (HRM3)**		HadCM3 (custom run for NARCCAP); Gordon (2000), Pope (2000).	T, T _{max} , T _{min} , P	12/1970 – 11/2000 12/2040 – 11/2070

*T – mean temperature; T_{max} – maximum temperature; T_{min} – minimum temperature; P – precipitation.

** Monthly data for these two RCMs were calculated from the original 3-hourly files, with a day corresponding to 06 UTC – 06 UTC.

Figures 1 and 2 illustrate the 1971-2000 annual mean temperature and precipitation fields, respectively, from an observed dataset (ANUSPLIN³) and derived from the driving GCM CGCM3 T47, two runs of the CRCM and a single run from RCM3 (both RCMs driven by CGCM3 T47) and a single run of HRM3 (driven by HadCM3). Comparison with the observed mean temperature climatology indicates that the two CRCM and single RCM3 run tend to be slightly cooler than observed, whilst HRM3 is slightly warmer. All RCMs indicate precipitation conditions which are slightly wetter than observed⁴. In contrast to the driving GCM, the higher elevation areas in the west are easily apparent in all RCM runs, picked out by lower temperatures and higher precipitation. It is also possible to identify higher elevation areas such as the Cypress Hills (Alberta-Saskatchewan border) in the precipitation fields of all RCMs, in particular with HRM3. The two CRCM runs (aet and aev) exhibit generally cooler mean temperatures than CGCM3 T47, while for RCM3 temperatures are similar. HRM3 is generally warmer than the other two RCMs, although the driving GCM is not available for comparison. For precipitation, the two CRCM fields exhibit similar values to the driving GCM, although the higher elevation areas are a lot wetter, while RCM3 is generally about 100-200 mm wetter and even more so in

³ Time series of climate data (maximum and minimum temperature, precipitation) gridded to a 0.083333° latitude/longitude resolution for the period 1901-2008 using the ANUSPLIN (thin-plate smoothing splines on geographic location and elevation) software were obtained from Dan McKenney at NRCan. Climate normals gridded using this methodology have been shown to perform well in the prairie ecozone, with temperatures generally being within 1°C and precipitation within several percent. Milewska *et al.* (2005) recommended ANUSPLIN grids for the mountains in south-eastern British Columbia and south-western Alberta, with temperature grids verifying well in summer and winter with upper air soundings (maximum temperature) and station vertical profiles (minimum temperature). ANUSPLIN grids were also very close to water balance estimates of precipitation computed from streamflow gauge measurements, although values tended to be slightly low (Milewska *et al.*, 2005).

⁴ The RCMs and GCMs used here have not been driven by observed boundary conditions, and therefore we would not expect them to simulate the same climate as observed. Even if observed boundary conditions had been used, the chaotic nature of climate means that model simulations may still deviate from observed conditions. However, at this time resolution, i.e., averaged over 30 years, we would expect a ‘good’ climate model to be able to simulate observed climate patterns and magnitudes, and this does appear to be the case with the climate models examined here.

western areas. Figures 3 and 4 indicate results averaged over the 2041-2070 period for mean temperature and precipitation, respectively. A similar pattern exists in this time period compared to 1971-2000, although mean temperatures are about 2°C warmer and precipitation totals are increased by about 100 mm. For the RCMs examined here, they certainly provide a more realistic picture of the climate over western Canada, particularly in the case of precipitation, when compared with the driving GCM.

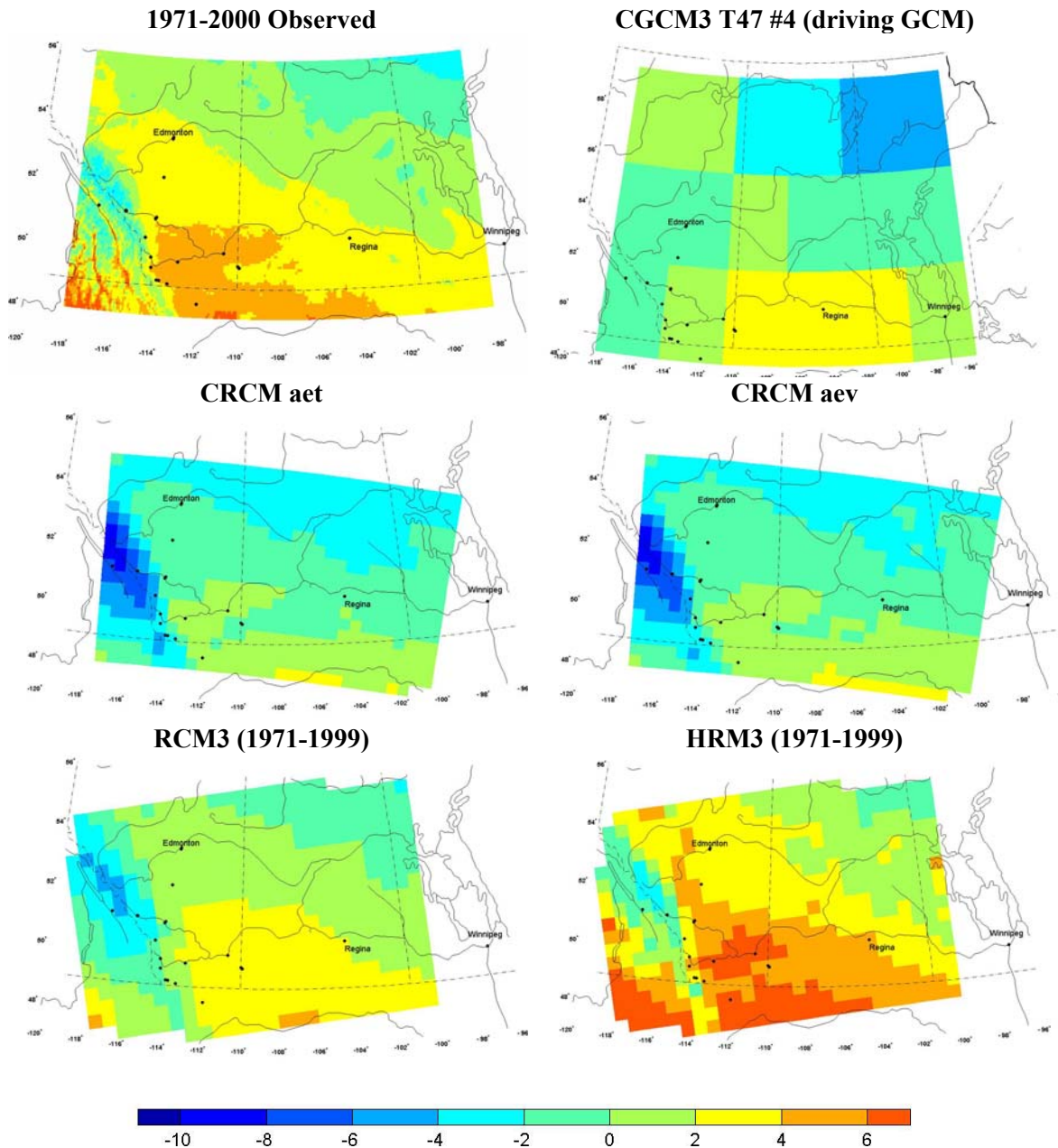


Figure 1: Representation of 1971-2000 mean annual temperature (°C). Note that HRM3 is driven with HadCM3 and not CGCM3 T47. Black dots represent the locations of stream gauge stations.

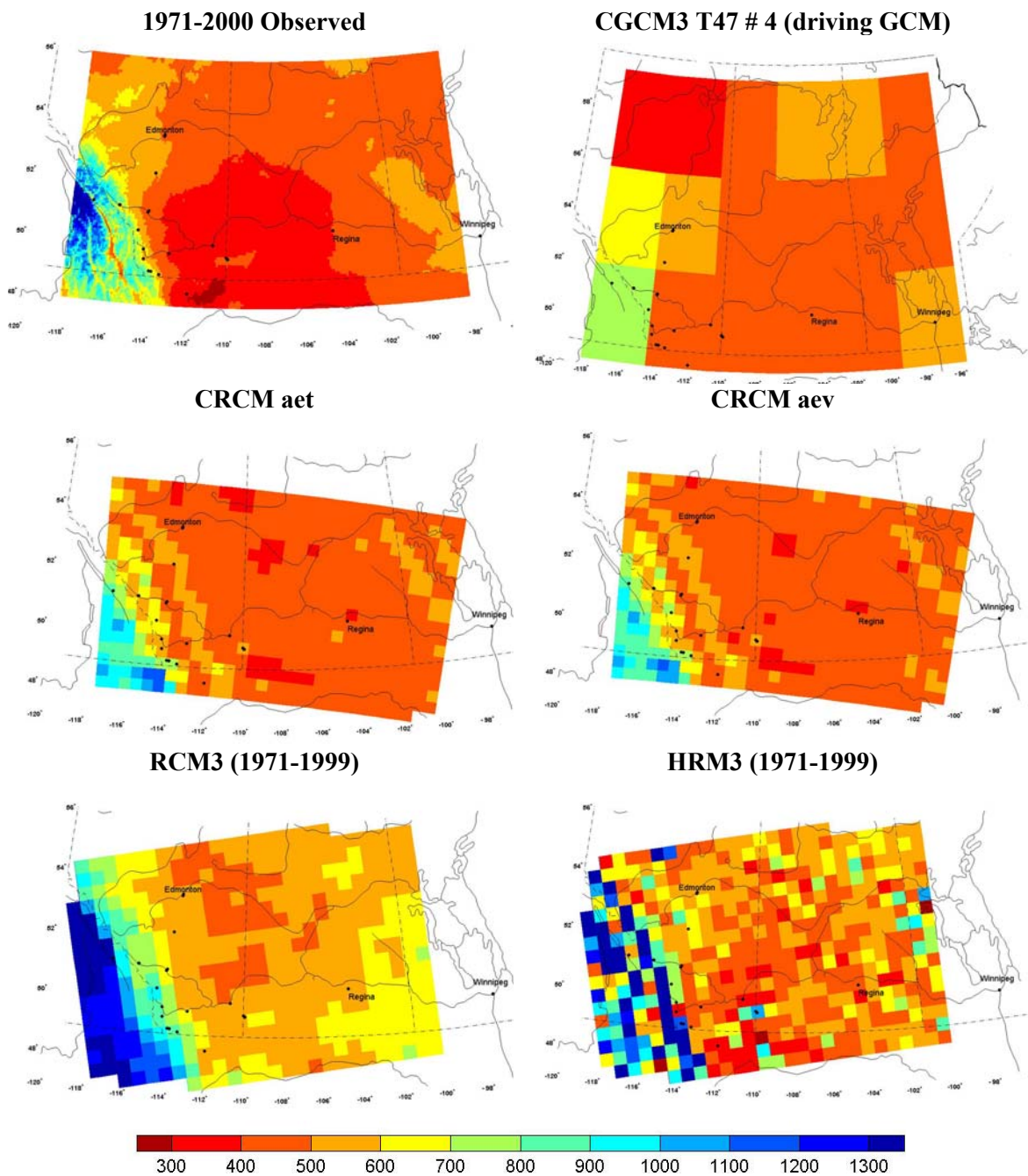


Figure 2: Representations of 1971-2000 annual precipitation totals (mm). Note that HRM3 is driven with HadCM3 and not CGCM3 T47. Black dots represent the locations of stream gauge stations.

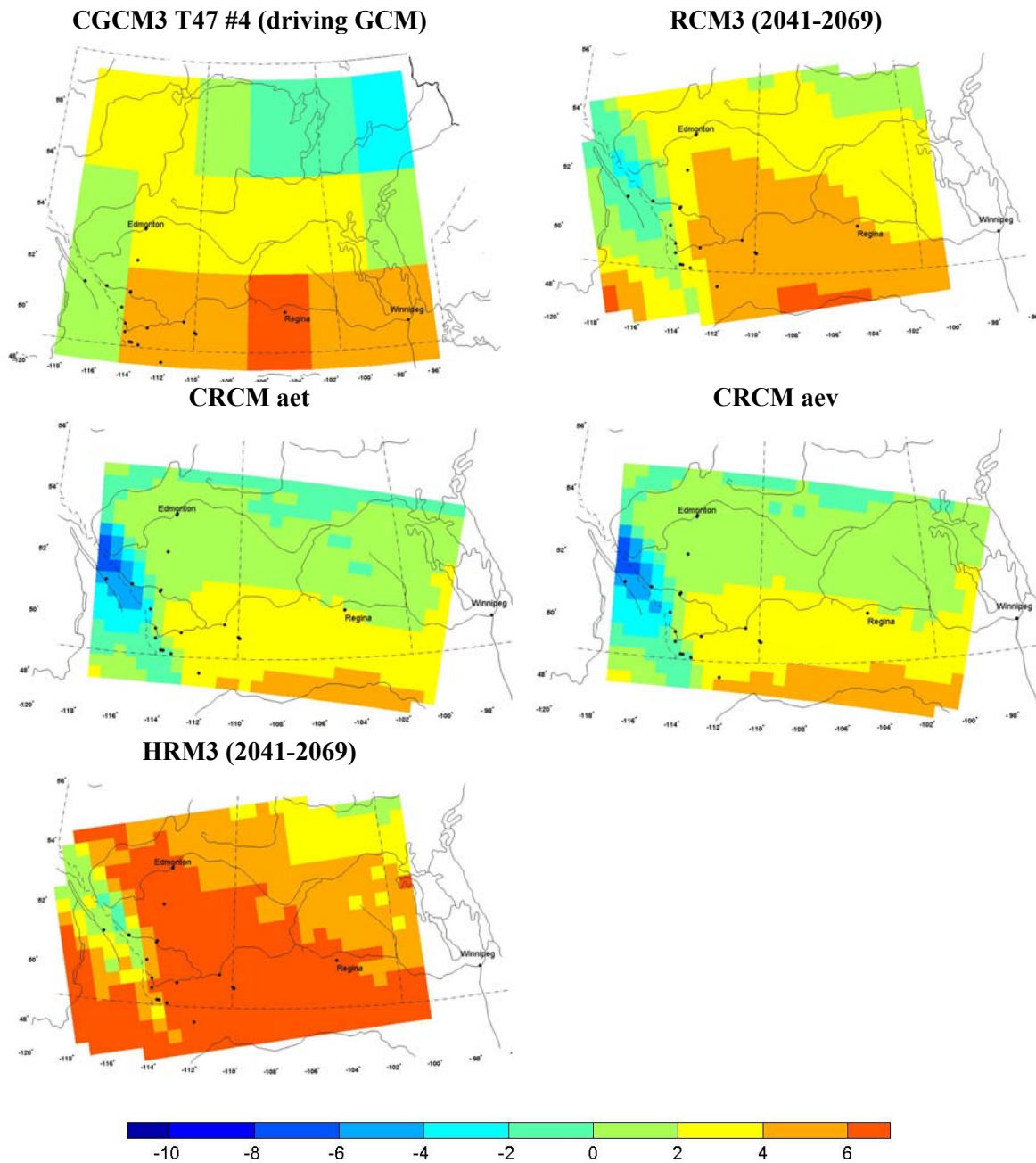


Figure 3: Representation of 2041-2070 mean annual temperature (°C). Note that HRM3 is driven with HadCM3 and not CGCM3 T47. Black dots represent the locations of stream gauge stations.

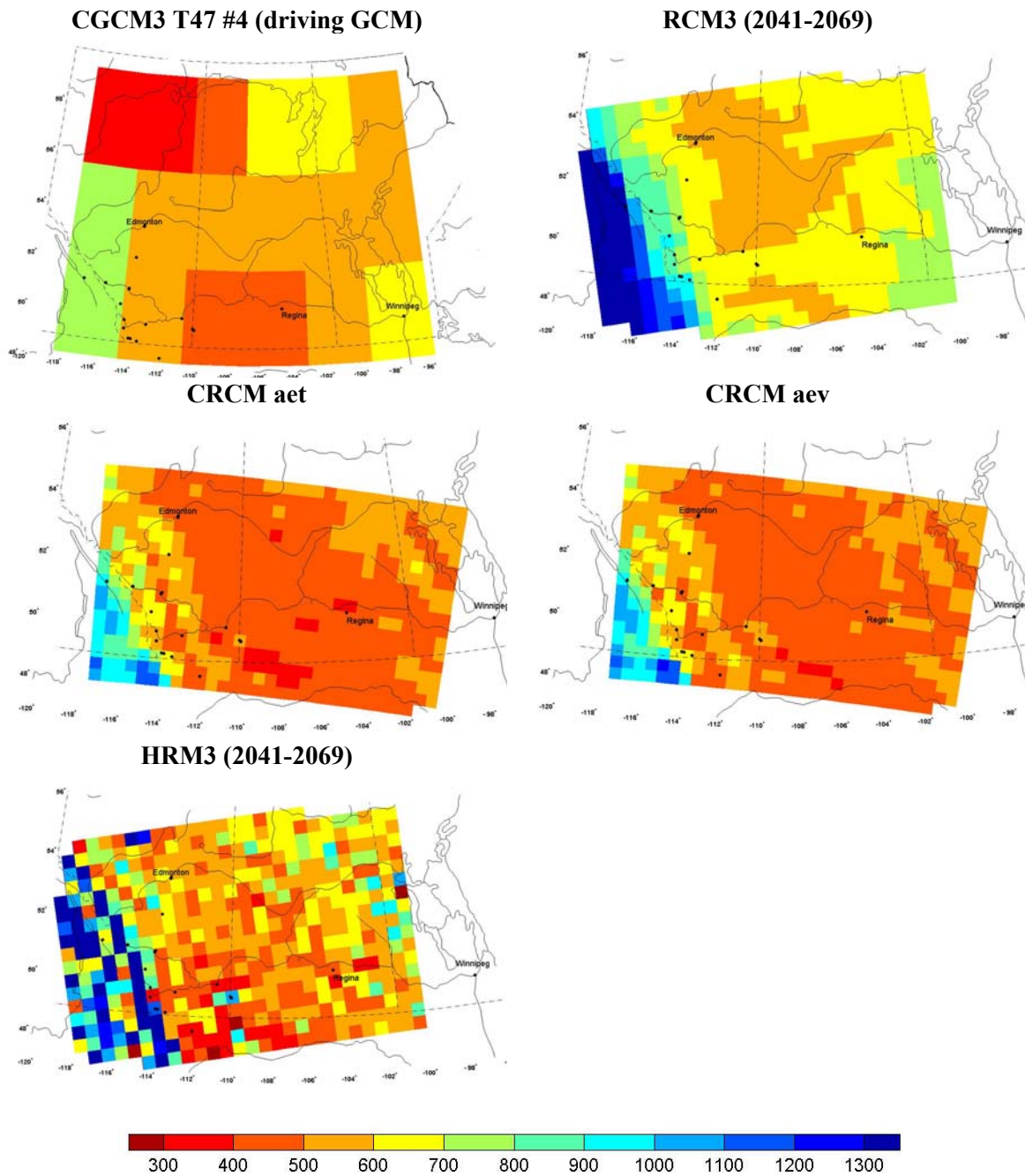


Figure 4: Representations of 2041-2070 annual precipitation totals (mm). Note that HRM3 is driven with HadCM3 and not CGCM3 T47. Black dots represent the locations of stream gauge stations.

Moisture deficits

Potential evapotranspiration (PET) and moisture deficit, also known as the climate moisture index (CMI) were then calculated from the gridded observed data (ANUSPLIN) and climate model output. CMI is a measure of effective precipitation in excess of water loss by evapotranspiration,

i.e., $P - PET$. Hogg (1994) has shown this index to be meaningful biogeographically, with a CMI value of zero (i.e., $P = PET$) defining the southern boundary of the boreal forest and a value of -15 corresponding to the aspen parkland–grassland boundary in western Canada (based on 1951-1980 climate data). Here, the CMI has been calculated for the water year (October to the following September) and also over the three-month period May, June and July. There are a number of different methods available for calculating potential evapotranspiration, all with associated advantages and disadvantages. The two reported here have been chosen for their relative simplicity and basic climate data requirements.

1. Thornthwaite method

The Thornthwaite method is based mainly on mean temperature with an adjustment being made for the number of daylight hours. An estimate of the PET (Shaw, 1994), calculated on a monthly basis, is given by:

$$PE_m = 16N_m \left(\frac{10\overline{T}_m}{I} \right)^a$$

where m is the months 1, 2, 3, ... 12, N_m is the monthly adjustment factor related to the hours of daylight, \overline{T}_m is the monthly mean temperature ($^{\circ}\text{C}$), I is the heat index for the year, given by:

$$I = \sum i_m = \sum \left(\frac{\overline{T}_m}{5} \right)^{1.5} \quad \text{for } m = 1 \dots 12$$

$$\text{and } a = 6.7 \times 10^{-7}I^3 - 7.7 \times 10^{-5}I^2 + 1.8 \times 10^{-2}I + 0.49$$

The Thornthwaite method of calculating PET tends to exaggerate PET and this is particularly marked in the summer months when high temperatures have a dominant effect in the calculation. The heat index, I , requires a full year's data for its calculation and missing data in any month therefore means that PET cannot be calculated for that particular year.

2. Simplified Penman-Monteith method

Hogg (1997) simplified the Penman-Monteith method of estimating potential evapotranspiration so that the only input required is the altitude of the station and the mean maximum and minimum temperature for each month. The monthly PET is calculated as:

$$\begin{aligned} \text{PET} &= 93 D \exp(A/9300) && \text{for } T > 10^{\circ}\text{C} \\ \text{PET} &= (6.2T+31)D \exp(A/9300) && \text{for } 10^{\circ}\text{C} > T > -5^{\circ}\text{C} \\ \text{PET} &= 0 && \text{for } T < -5^{\circ}\text{C} \end{aligned}$$

where PET is potential evapotranspiration (mm/month), T is mean temperature ($^{\circ}\text{C}$), D is vapour pressure deficit (kPa; $D = 0.5(e_{T_{\max}} + e_{T_{\min}}) - e_{T_{\text{dew}}}$), A is station altitude (m) and $e_{T_{\text{dew}}}$ is equivalent to the saturation vapour pressure at 2.5°C below mean minimum temperature.

Figures 5-8 illustrate the 1971-2000 and 2041-2070 mean potential evapotranspiration fields calculated using the Thornthwaite (Figures 5 and 6) and the simplified Penman methods (Figures 7 and 8). Maximum and minimum temperature were not available for CGCM3 T47 and altitude was not available for HRM3, so calculation of PET using the simplified Penman method was not possible for these two models. On comparing the two observed annual PET fields, it is apparent that the Thornthwaite method results in larger totals (generally between about 500 and 600 mm) than those of the simplified Penman method (generally between 300 and 400 mm, but between

400 and 500 mm in the south). For the Thornthwaite PET fields, the driving GCM, the two CRCM runs and the RCM3 run underestimate annual PET by about 100 mm. The HRM3 simulation shows a similar picture to the 1971-2000 normal, although there are areas in the far south of the region where PET totals are about 100 mm too high. The simulations for the 2041-2070 period all indicate increases in annual PET totals (of about 100 mm), although the largest increases occur in the HRM3 simulation.

In contrast, use of the simplified Penman method for calculating PET results in larger potential evapotranspiration totals than observed for the two CRCM runs (Figure 7). In the northern half of the region, totals are about 100 mm greater than observed for these two runs, whilst in the south PET totals are as much as 300 mm greater than observed. For RCM3, however, the opposite is the case, i.e., annual PET totals are generally about 100 mm lower than observed. One of the reasons for this may be that RCM3's representation of mean maximum temperature is cooler than that of the other RCMs, by about 2°C on an annual basis, and by about 4°C in summer months when potential evapotranspiration is at its greatest (see Figures 9 and 10). PET is greater in the 2041-2070 time period (Figures 6 and 8), as would be expected given the projected increase in temperature over time, but larger increases are apparent with the simplified Penman method (≈ 200 mm) compared to the Thornthwaite method (≈ 100 mm). This is likely driven by the inclusion of maximum temperature in the simplified Penman method.

Moisture deficits (P-PET) were calculated for the water year (October to the following September) and for a three-month period, May-June-July, and maps for these are shown in Figures 11 to 18. On comparison, the two methods of calculating PET result in very similar pictures of observed annual moisture deficits. The main difference is an area of more intense moisture deficit (about 100 mm greater) in eastern Alberta and along the provincial border with Saskatchewan, as well as along the international border with the USA, in the results obtained using the simplified Penman method of calculating PET (Figure 13). Figure 11 indicates that, for moisture deficits calculated using the Thornthwaite method, the driving GCM and the two CRCM runs illustrate similar results as the observed climatology, although the modelled area of deficit extends slightly further north than in the observed picture. The RCM3 simulation shows almost no areas of moisture deficit on an annual basis, while HRM3 tends to exaggerate the deficits when compared to observed. For the 2041-2070 period, all models, with the exception of RCM3, show increases in intensity and in area of moisture deficit (Figure 12). For the future period, RCM3 shows no areas of deficit in annual moisture. This result for RCM3 is also the same when PET has been calculated using the simplified Penman method (Figures 13 and 14). Annual moisture deficits calculated using the simplified Penman methodology indicate that the two CRCM simulations show a larger area of moisture deficit when compared with the 1971-2000 climatology (Figure 13), with deficit values generally being between 0 and 200 mm, and between 200 and 400 mm in the south. For the future time period (Figure 14) deficits increase by about 200 mm, so that they are generally between 200 and 400 mm, and between 400 and 600 mm in the south.

Summer (May-June-July) moisture deficits are illustrated in Figures 15-18. The Thornthwaite method of calculating PET results in a larger area of more intense observed summer moisture deficit (generally between about 100 and 200 mm; Figure 15) than that of the simplified Penman method (Figure 17), where deficits of this magnitude are confined to the southern half of Alberta and Saskatchewan. Model simulations of summer moisture deficit generally indicate less intense deficits than observed, with the RCM3 simulation being too wet regardless of the method used to calculate PET. For the CRCM and HRM3 simulations, the future picture is one of more intense moisture deficits in summer.

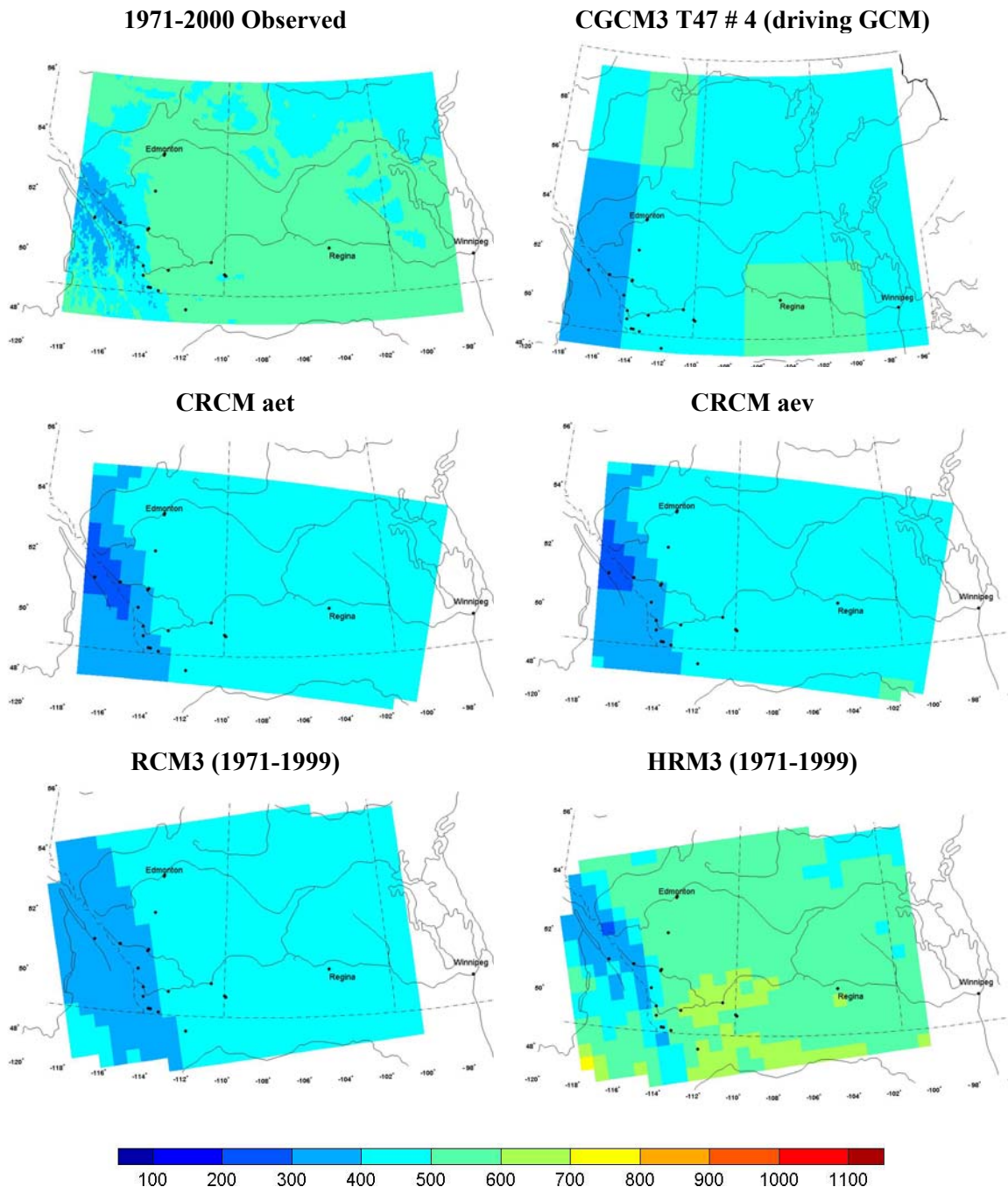


Figure 5: Representations of 1971-2000 annual potential evapotranspiration totals (mm) calculated using the Thornthwaite method. Note that HRM3 is driven with HadCM3 and not CGCM3 T47. Black dots represent the locations of stream gauge stations.

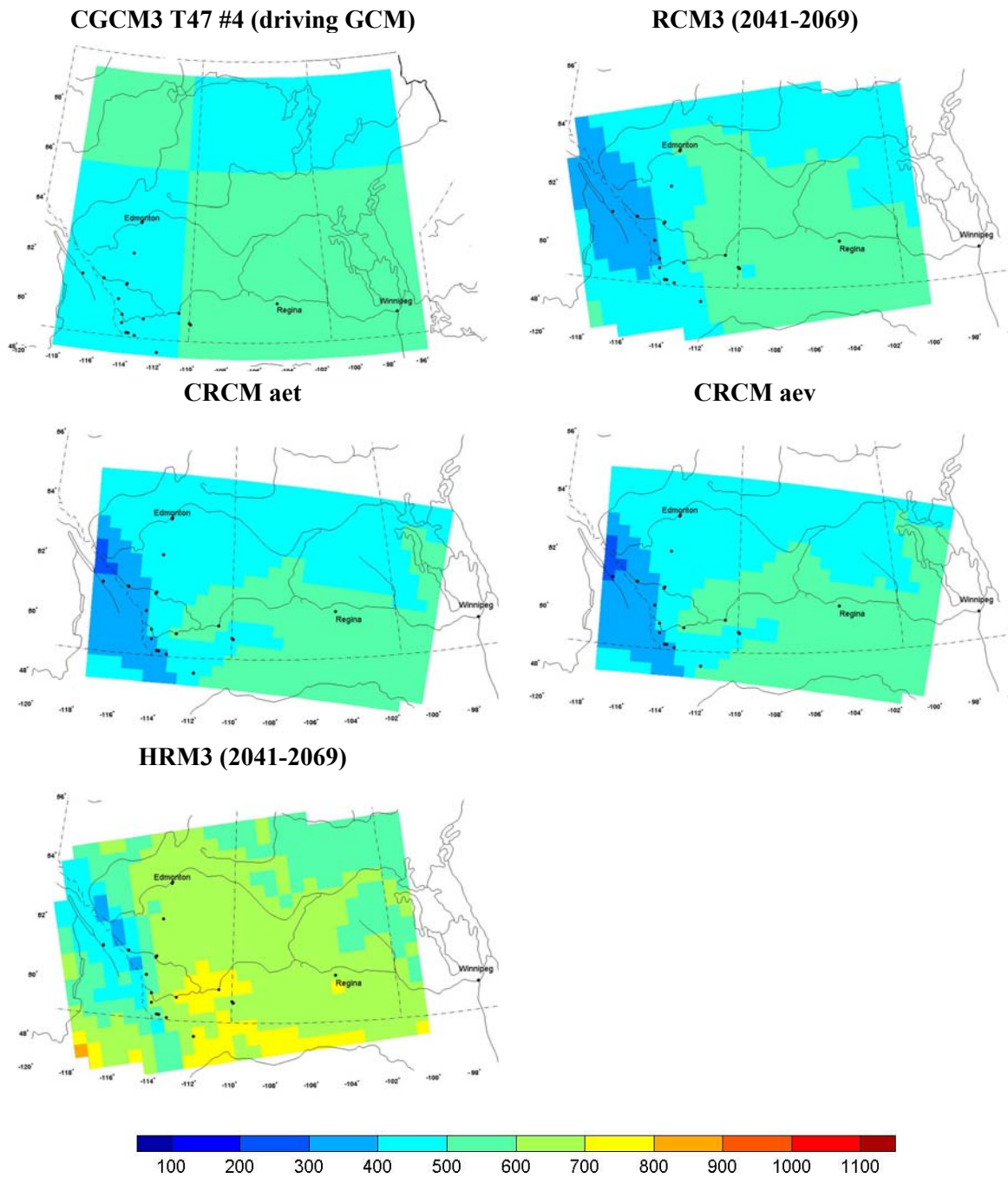


Figure 6: Representations of 2041-2070 annual potential evapotranspiration totals (mm) calculated using the Thornthwaite method. Note that HRM3 is driven with HadCM3 and not CGCM3 T47. Black dots represent the locations of stream gauge stations.

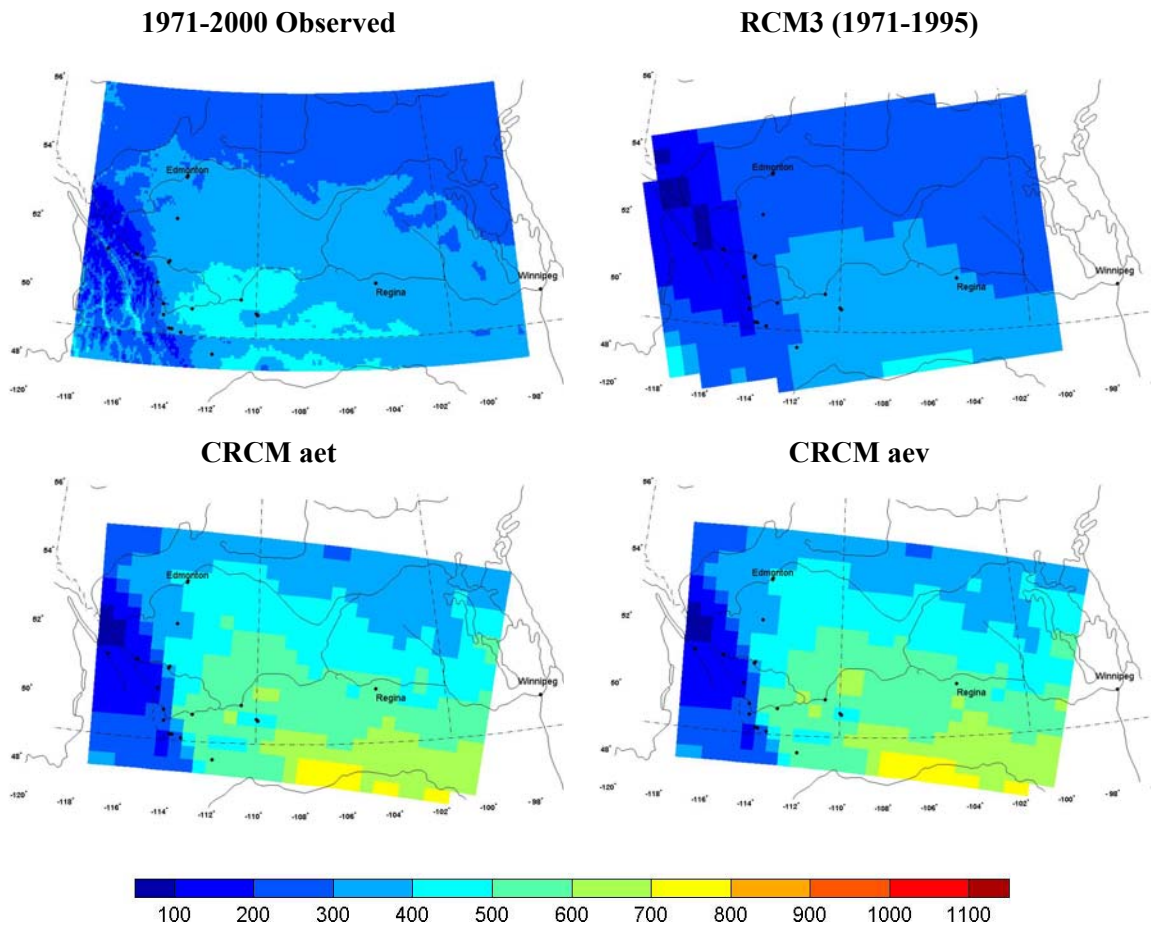


Figure 7: Representations of 1971-2000 annual potential evapotranspiration totals (mm) calculated using the simplified Penman method. Black dots represent the locations of stream gauge stations.

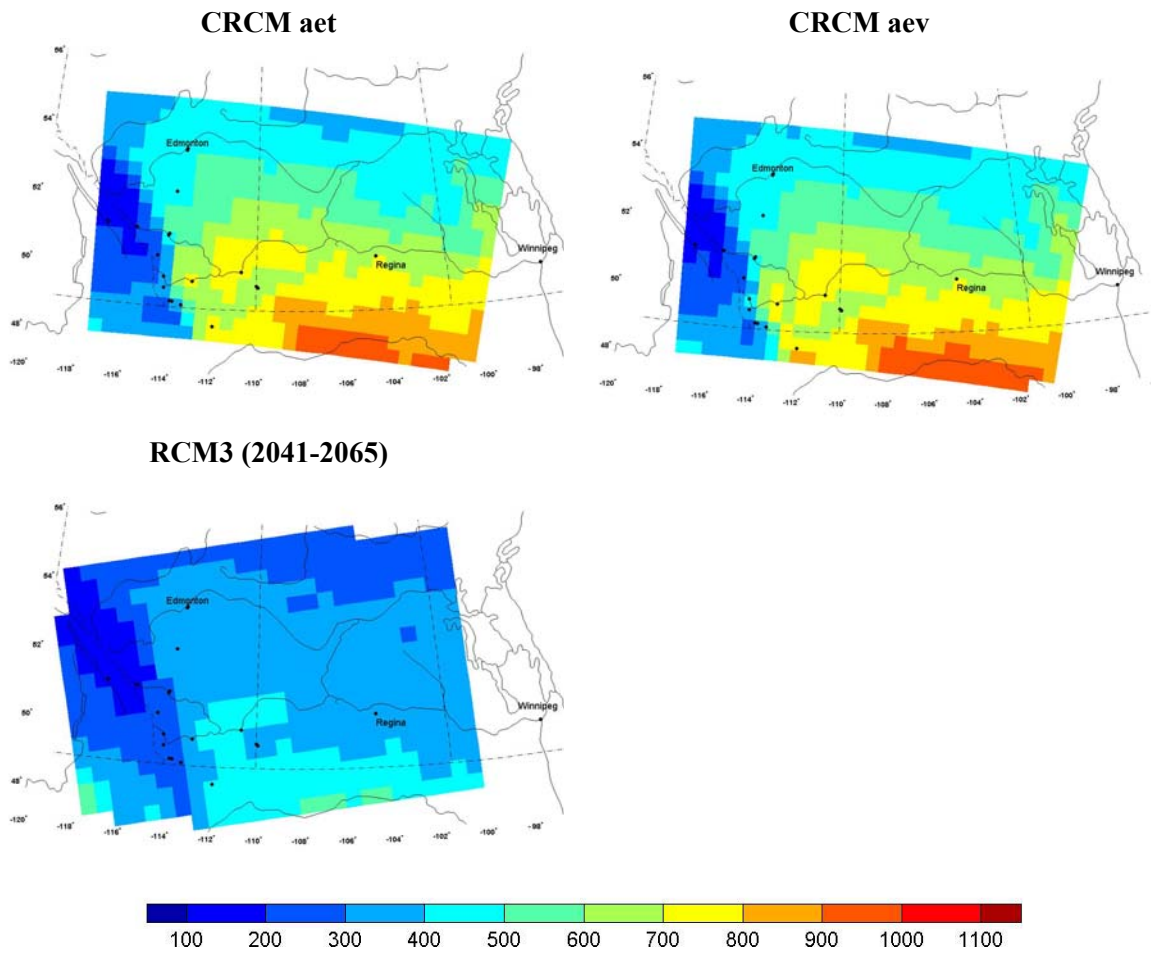


Figure 8: Representations of 2041-2070 annual potential evapotranspiration totals (mm) calculated using the simplified Penman method. Black dots represent the locations of stream gauge stations.

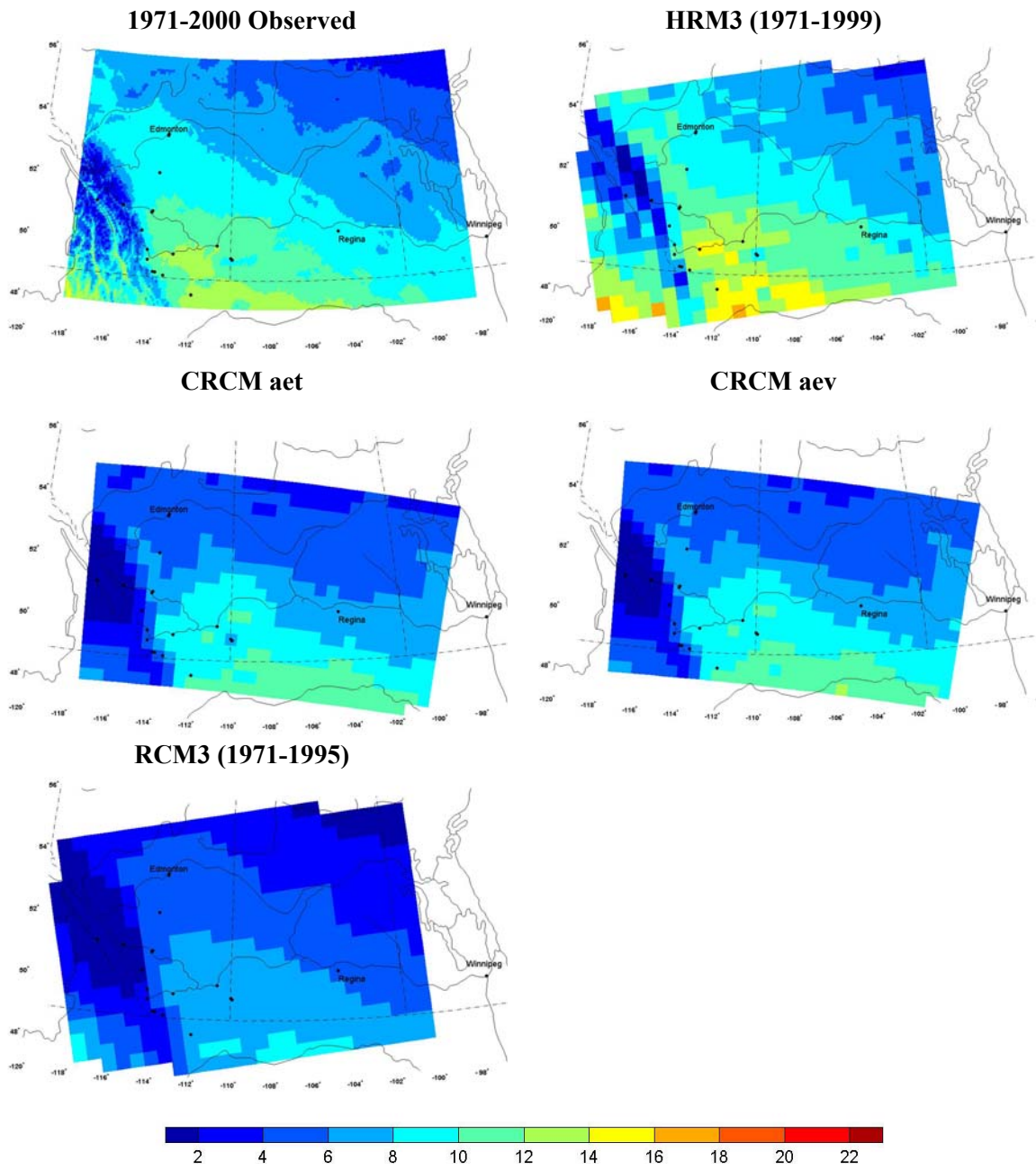


Figure 9: Representations of 1971-2000 annual mean maximum temperature (°C). Note that HRM3 is driven with HadCM3 and not CGCM3 T47. Black dots represent the locations of stream gauge stations.

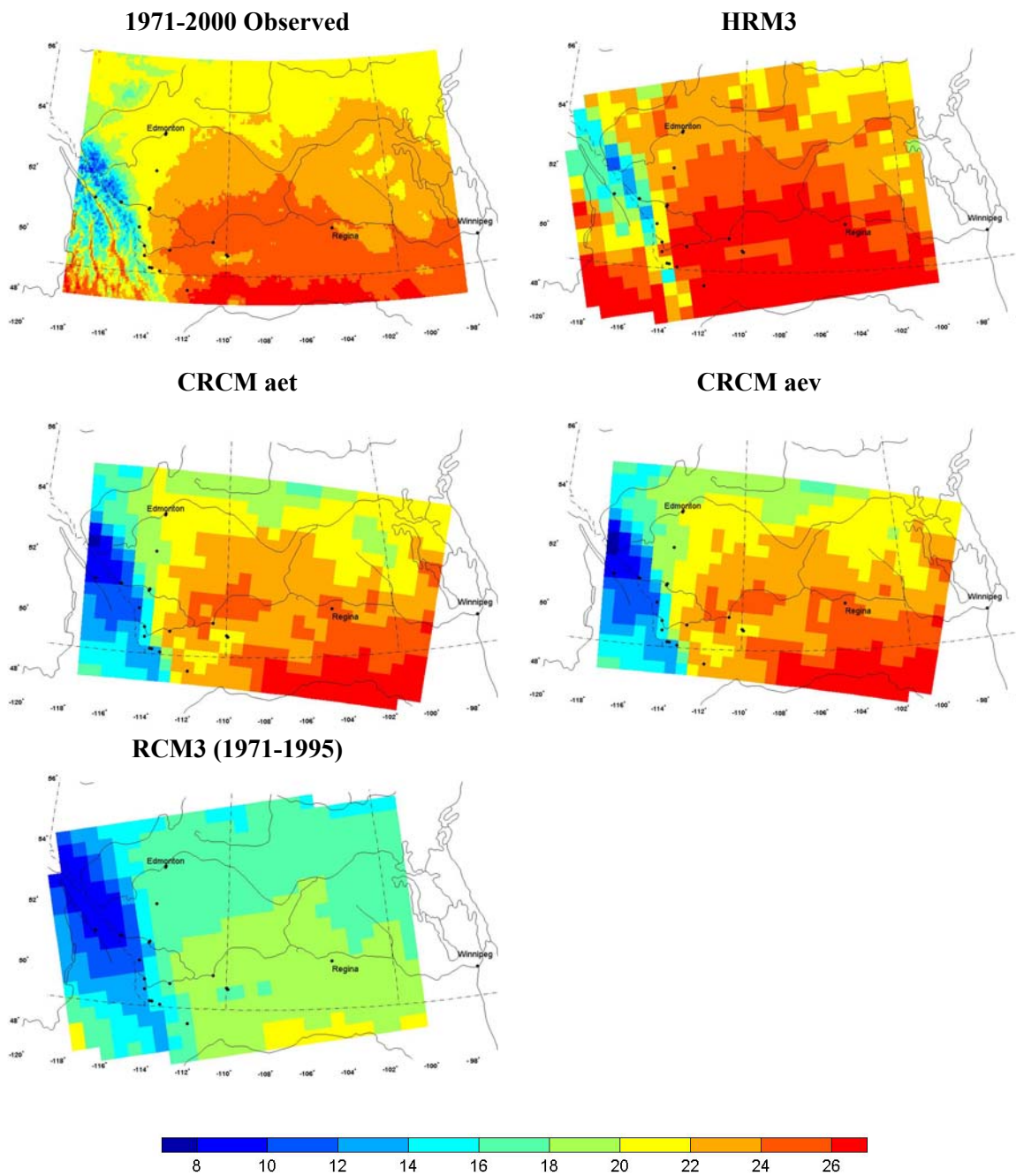


Figure 10: Representations of 1971-2000 summer (JJA) mean maximum temperature ($^{\circ}\text{C}$). Note that HRM3 is driven with HadCM3 and not CGCM3 T47. Black dots represent the locations of stream gauge stations.

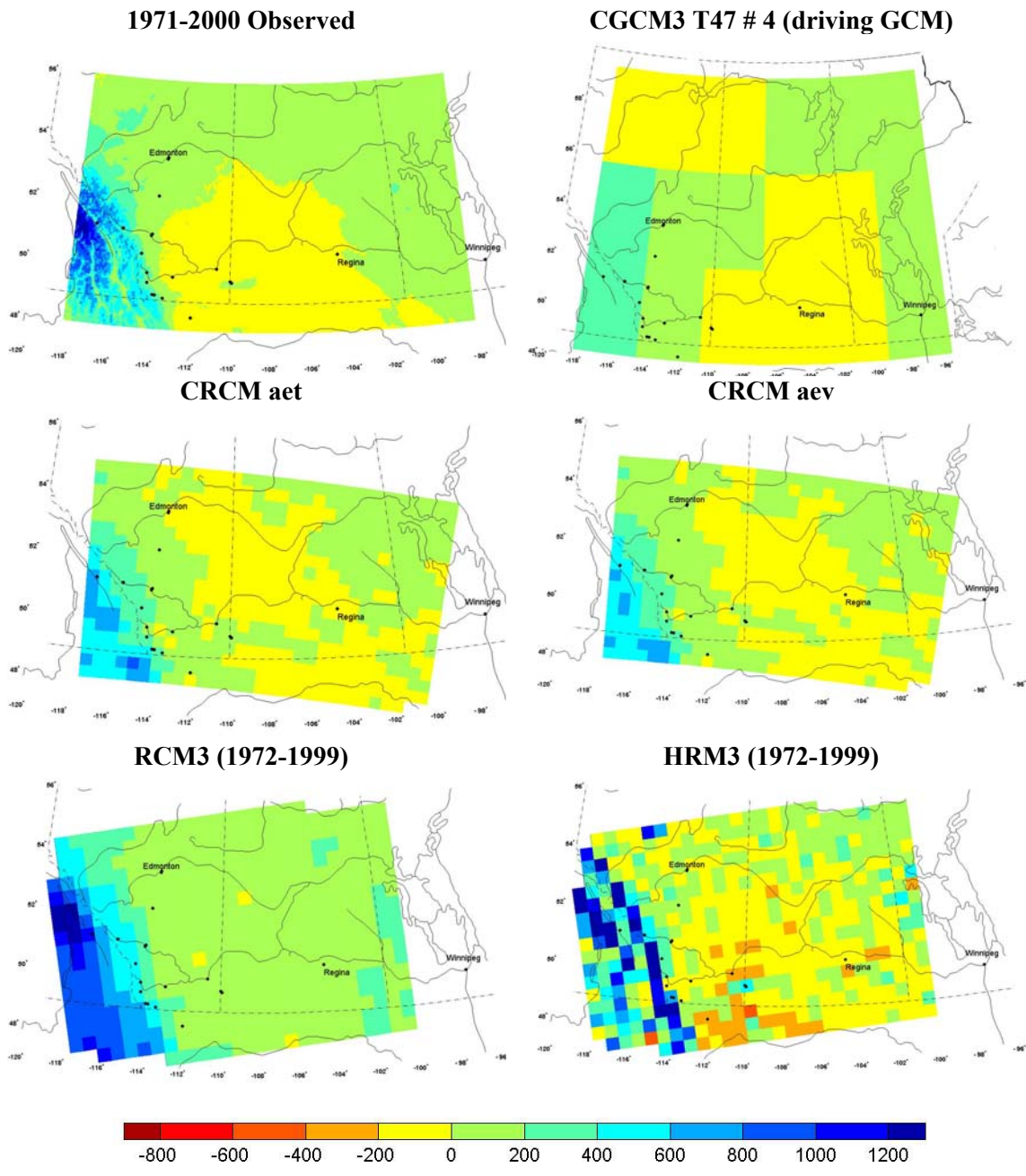


Figure 11: Representations of 1971-2000 total annual moisture deficit (mm) for the water year (October – September), with PET calculated using the Thornthwaite method. Note that HRM3 is driven with HadCM3 and not CGCM3 T47. Black dots represent the locations of stream gauge stations.

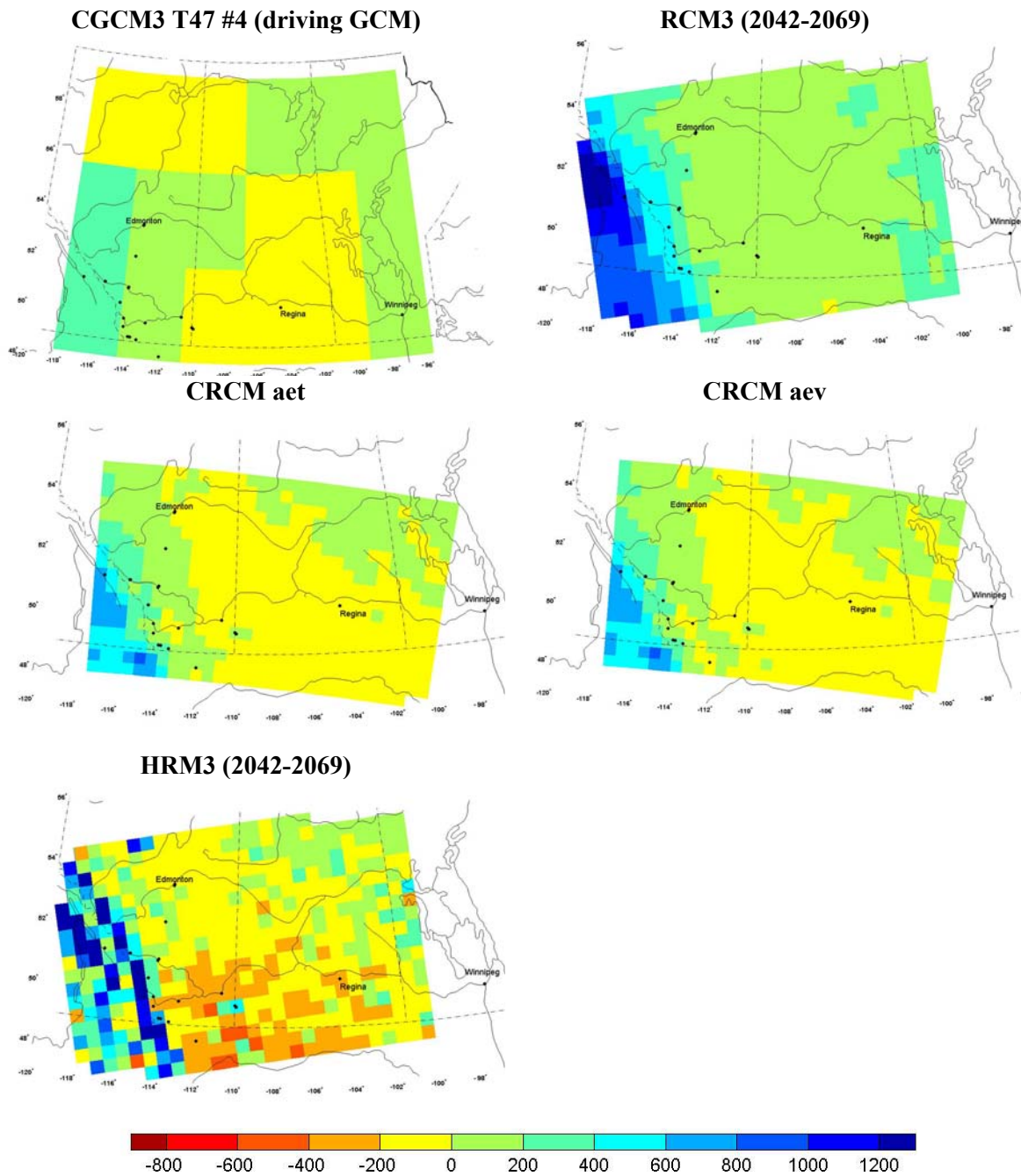


Figure 12: Representations of 2041-2070 total annual moisture deficit (mm) for the water year (October – September), with PET calculated using the Thornthwaite method. Note that HRM3 is driven with HadCM3 and not CGCM3 T47. Black dots represent the locations of stream gauge stations.

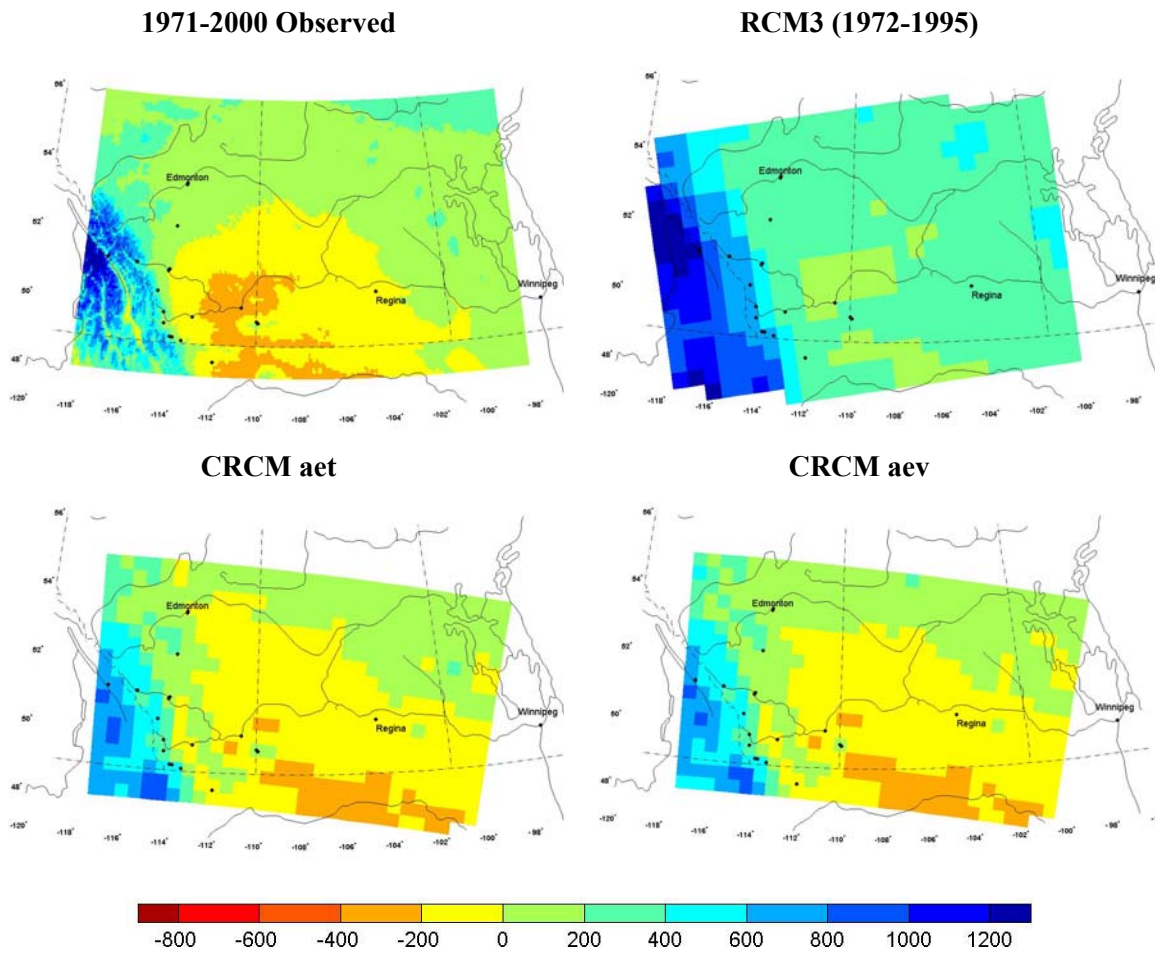


Figure 13: Representations of 1971-2000 total annual moisture deficit (mm) for the water year (October – September), with PET calculated using the simplified Penman method. Black dots represent the locations of stream gauge stations.

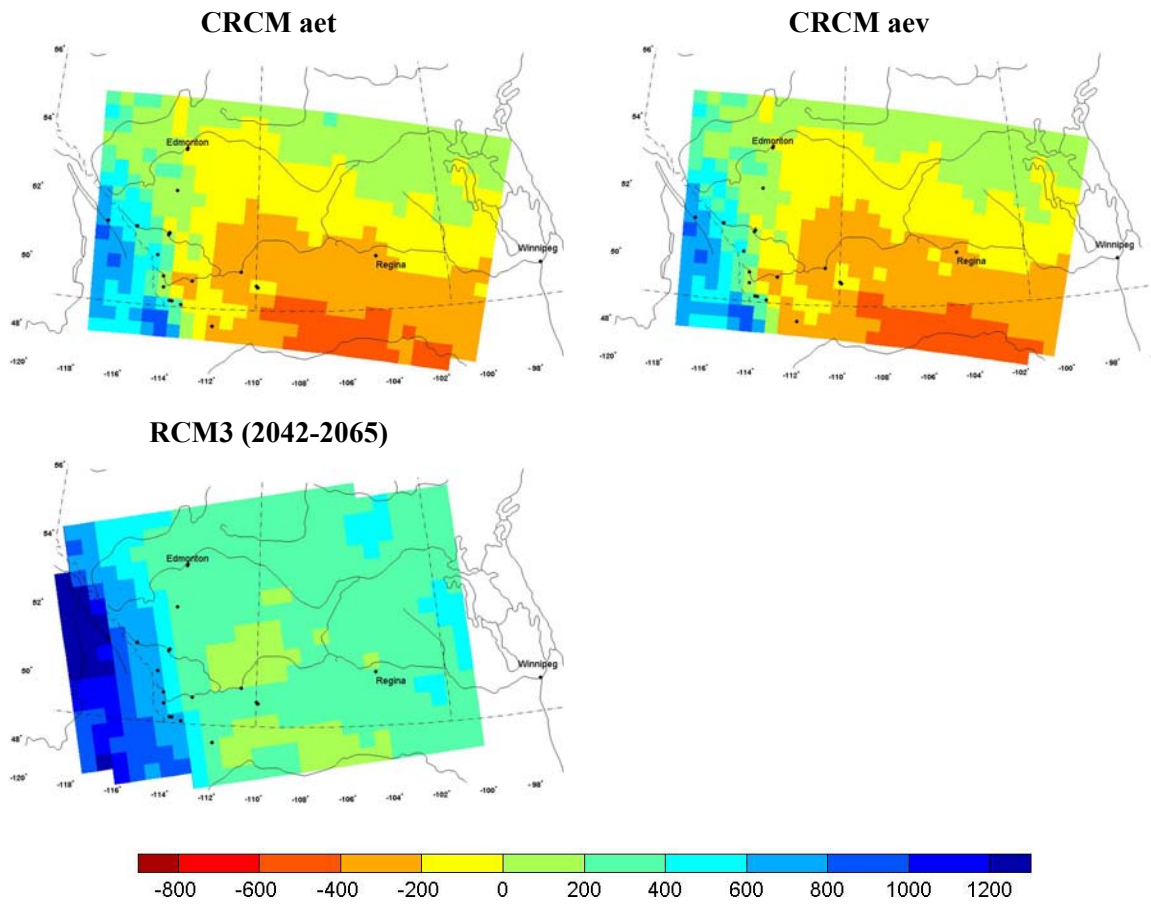


Figure 14: Representations of 2041-2070 total annual moisture deficit (mm) for the water year (October – September), with PET calculated using the simplified Penman method. Black dots represent the locations of stream gauge stations.

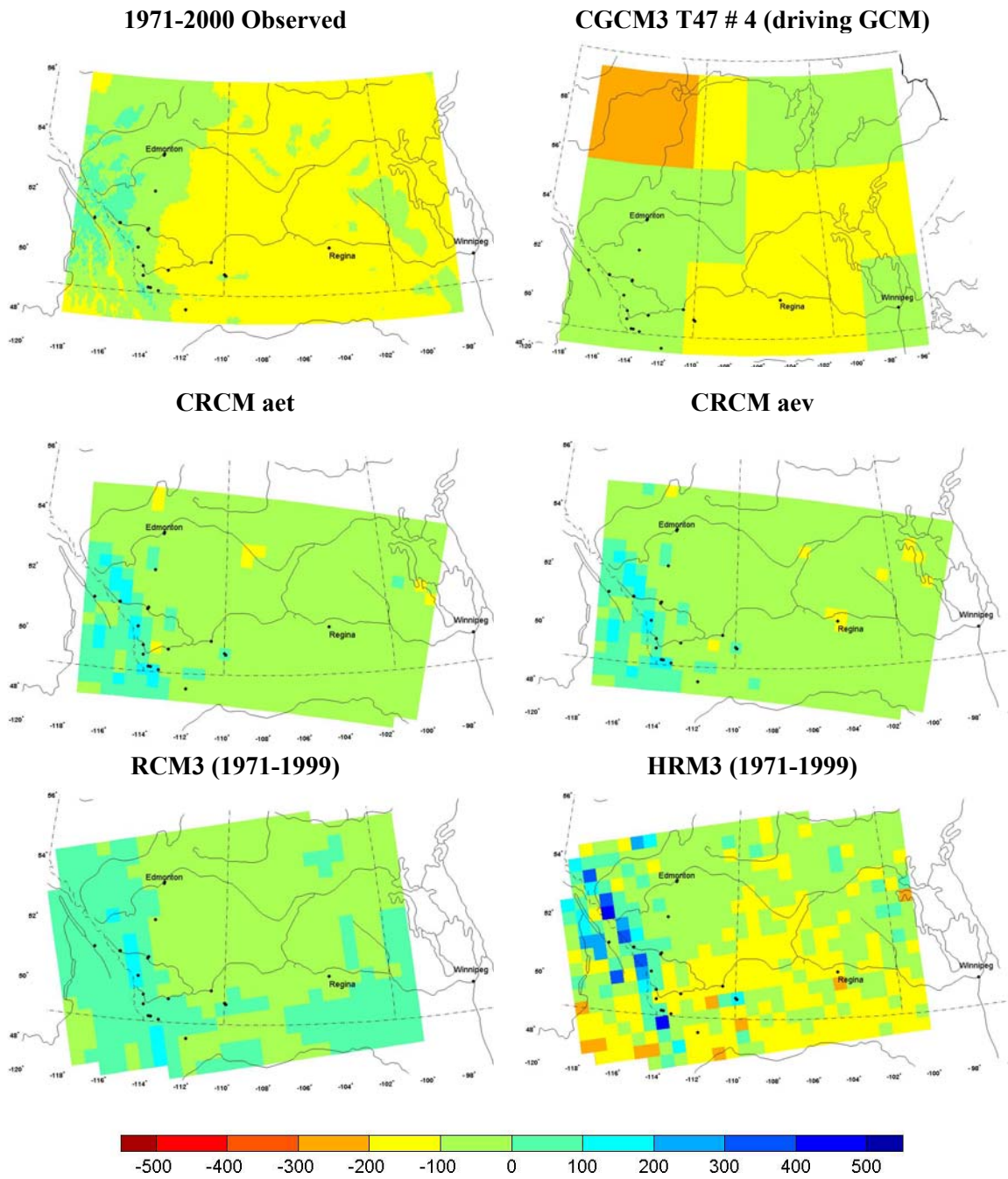


Figure 15: Representations of 1971-2000 May-June-July moisture deficit (mm), with PET calculated using the Thornthwaite method. Note that HRM3 is driven with HadCM3 and not CGCM3 T47. Black dots represent the locations of stream gauge stations.

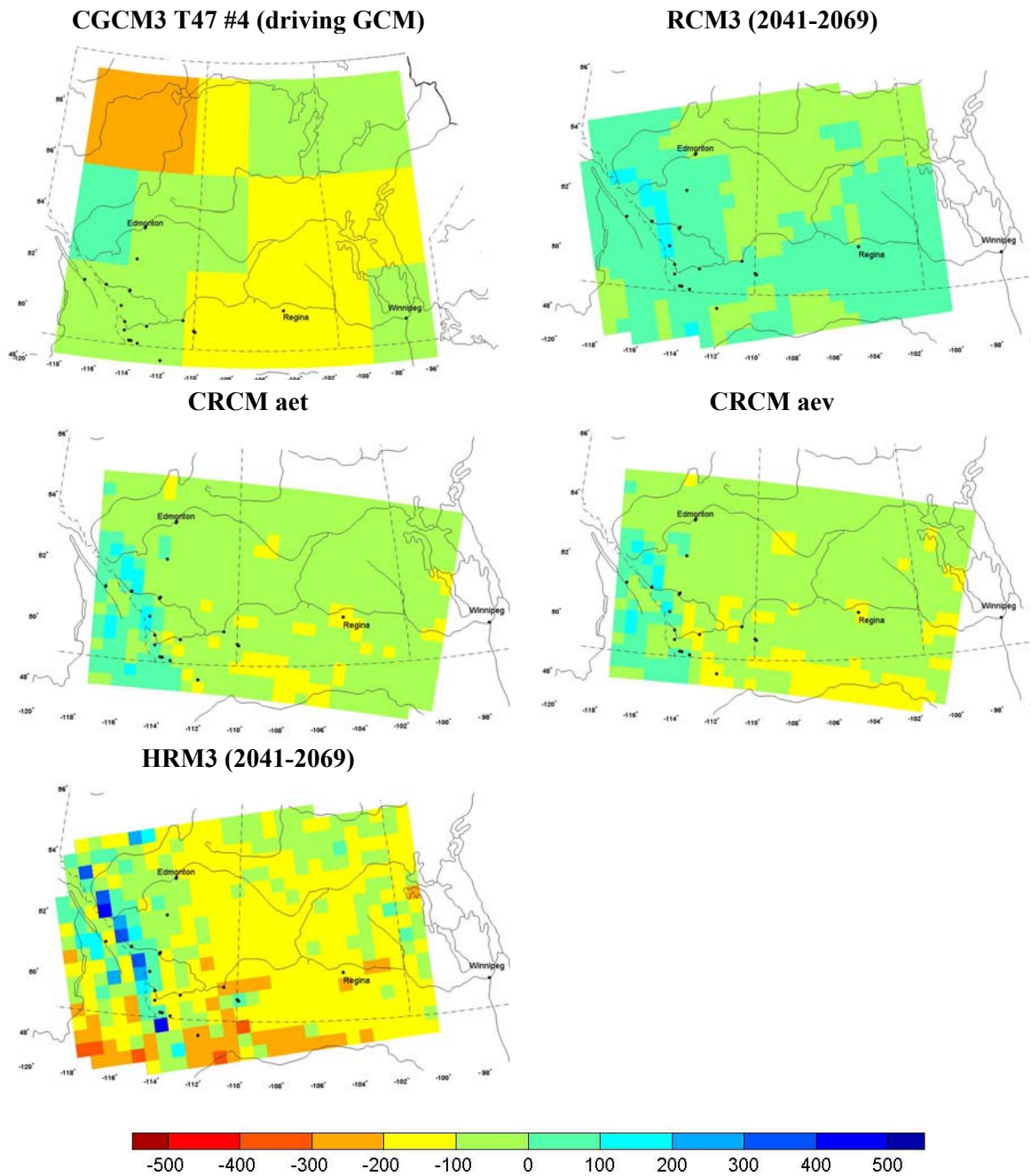


Figure 16: Representations of 2041-2070 May-June-July moisture deficit (mm), with PET calculated using the Thornthwaite method. Note that HRM3 is driven with HadCM3 and not CGCM3 T47. Black dots represent the locations of stream gauge stations.

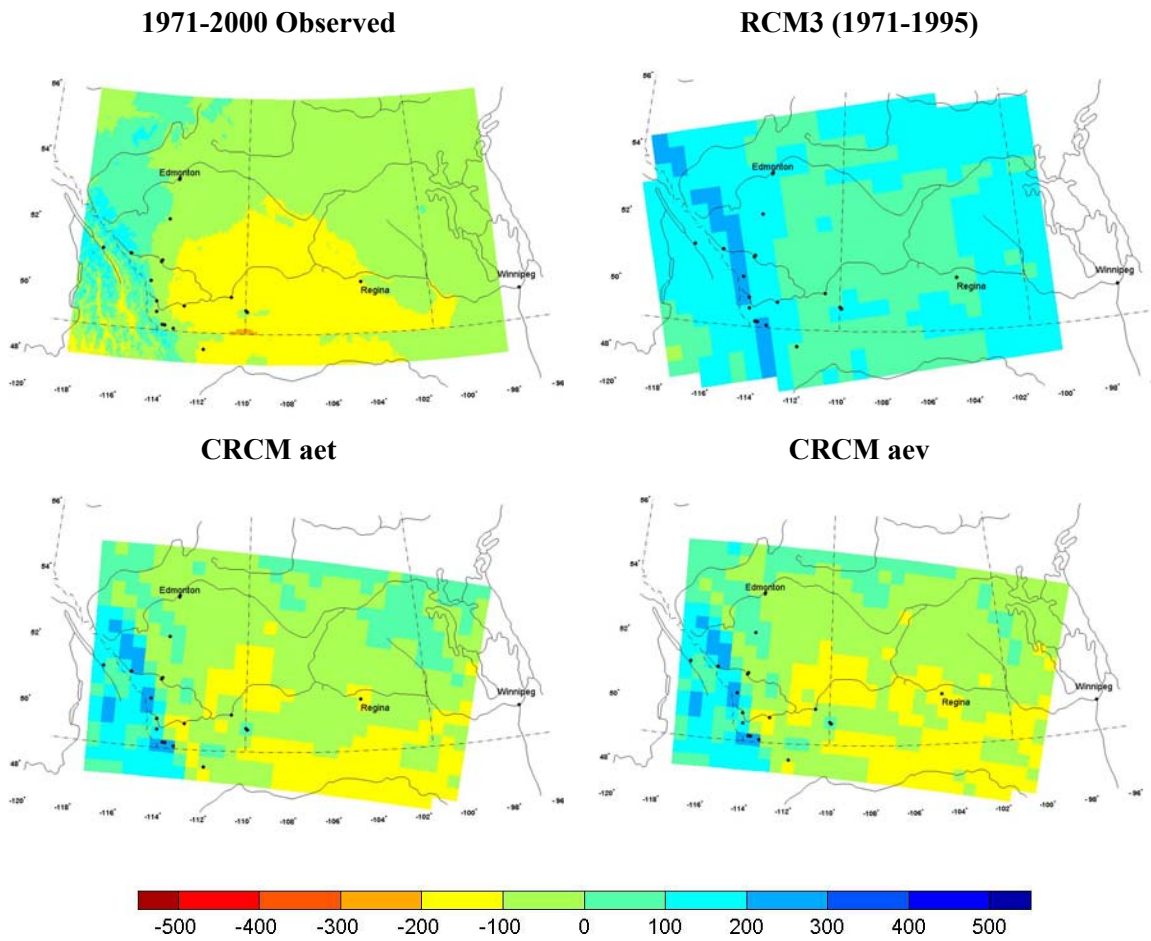


Figure 17: Representations of 1971-2000 May-June-July moisture deficit (mm), with PET calculated using the simplified Penman method. Black dots represent the locations of stream gauge stations.

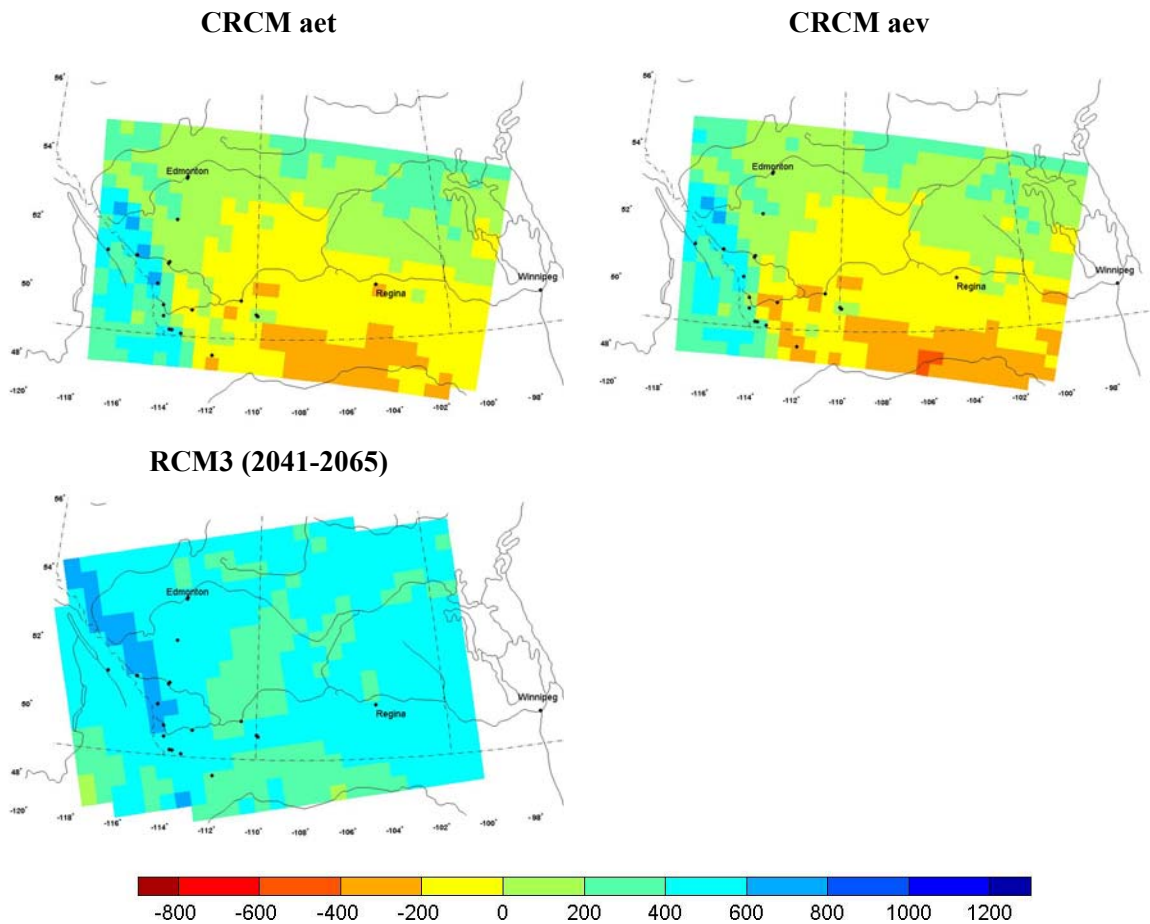


Figure 18: Representations of 2041-2070 May-June-July moisture deficit (mm), with PET calculated using the simplified Penman method. Black dots represent the locations of stream gauge stations.

A more in-depth look at hydroclimate –an analysis at stream gauge locations

The above analysis has focussed on present and future mean (over 30 years) climate and so provides a snapshot of average climate. In this section, a more in-depth approach is taken to examine trends over time in hydroclimate at specific locations. St. Jacques *et al.* (2010) undertook an analysis of Northern Rocky Mountain streamflow records in order to determine the effects of the Pacific Decadal Oscillation (Mantua *et al.*, 1997) on stream flow variability in western Canada and to provide projections for the future. Here hydroclimate variables were examined at some of the stream gauges used by St. Jacques *et al.* (2010). These are listed in Table 3. Time series data were simply extracted from the grid box containing the gauge from the observed gridded time series, the driving GCM, CGCM3 T47, the two CRCM simulations and the single simulations from RCM3 and HRM3. In addition to the hydroclimate variables described above, surface runoff was also available from CGCM3 T47 and the two CRCM simulations. Of the eighteen gauges listed in Table 3, six were selected for display in this report: Bow at Banff (gauge 2), Elbow (gauge 9), Bow at Calgary (gauge 11), North Saskatchewan (gauge 12), Marias (gauge 13) and Battle (gauges 17 and 18).

Figure 19 illustrates annual potential evapotranspiration for these six gauges for the period 1960-2100. All gauges show an increase in annual PET over time, as would be expected with the projected increase in temperature. For the period 1960-2000 the simulations shown here generally tend to underestimate observed PET. For the gauges illustrated here, the largest increases in annual PET are projected to occur at the Marias and Battle stations – variability is also largest at these two sites.

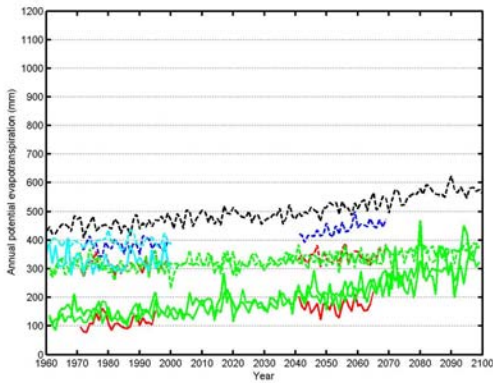
For annual moisture deficit (Figure 20), trends to more severe deficits in the future are most apparent for the two CRCM simulations, although the driving GCM, CGCM3 T47, exhibits little or no trend over the whole 1960-2100 period (but exhibits moisture surplus rather than deficit). A similar picture exists for summer moisture deficits (Figure 21), although in this case the driving GCM tends to exhibit moisture deficit over most of the time period. It is difficult to determine trends for the two RCMs, HRM3 and RCM3, since the time series are too short.

For surface runoff, the only gauge which exhibits a decreasing trend into the future is at the Bow River at Banff, where variability in runoff is also high (Figure 22). For the other five gauges, there is little difference between the driving GCM and the two CRCM runs and totals and variability are much lower than for the Bow River at Banff.

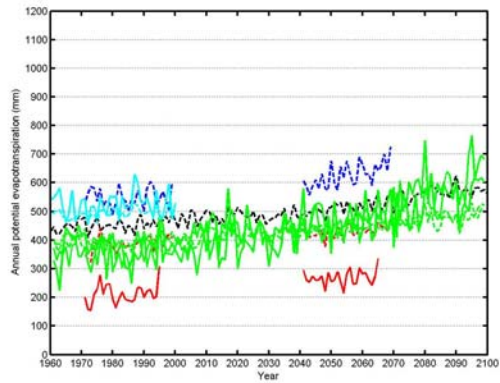
Table 3: Location of stream gauge stations and corresponding grid boxes for each RCM and the driving AOGCM CGCM3 T47. Colours indicate when gauges are in the same grid box.

	Gauge Name	Lat (°N)	Lon (°W)	CGCM3		CRCM		RCM3		HRM3	
				°N	°W	°N	°W	°N	°W	°N	°W
1	Waterton	49.11	113.83	50.1	112.5	48.98	113.55	49.05	113.58	49.16	113.94
2	Bow at Banff	51.17	115.57	50.1	116.25	51.29	115.31	51.03	115.72	51.21	115.38
3	Columbia	51.24	116.91	50.1	116.25	51.27	117.16	51.24	117.28	51.42	116.91
4	Red Deer	52.28	113.82	53.81	112.5	52.45	114.04	52.21	113.94	52.36	113.63
5	St. Mary	49.01	113.30	50.1	112.5	48.98	113.55	49.05	113.58	49.25	113.29
6	Belly	49.10	113.70	50.1	112.5	48.98	113.55	49.05	113.58	49.16	113.94
7	Oldman	49.71	112.86	50.1	112.5	49.73	112.93	49.58	113.05	49.77	112.76
8	S. Sask.	50.04	110.68	50.1	112.5	50.02	110.52	49.91	110.32	50.02	110.75
9	Elbow	51.01	114.09	50.1	112.5	50.90	114.08	50.80	114.18	50.97	113.86
10	Spray	51.16	115.55	50.1	116.25	51.29	115.31	51.03	115.72	51.21	115.38
11	Bow Calgary	51.05	114.05	50.1	112.5	50.90	114.08	50.80	114.18	50.97	113.86
12	N. Sask.	53.54	113.49	53.81	112.5	53.61	113.35	53.61	113.70	53.74	113.38
13	Marias	48.43	111.89	50.1	112.5	48.55	111.85	48.34	111.97	48.56	111.71
14	Waldron	49.81	114.18	50.1	112.5	49.75	114.11	49.82	114.55	50.02	114.24
15	Castle	49.49	114.14	50.1	112.5	49.37	114.12	49.39	114.40	49.59	114.09
16	Highwood	50.41	114.50	50.1	116.25	50.52	114.70	50.26	114.71	50.45	114.39
17	Battle	49.60	109.92	50.1	108.75	49.61	109.98	49.47	110.20	49.66	109.96
18	moved gauge	49.65	110.00	50.1	108.75	49.61	109.98	49.47	110.20	49.66	109.96

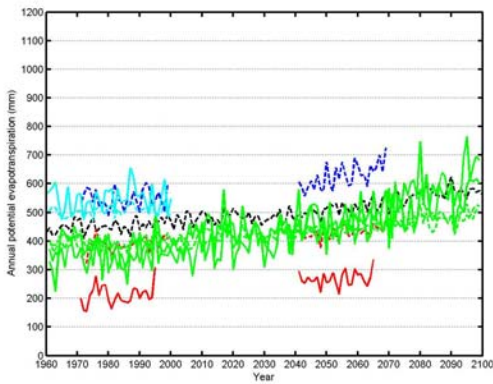
Bow at Banff (Gauge 2)



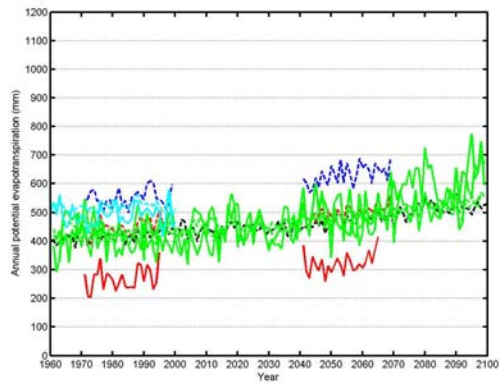
Elbow (Gauge 9)



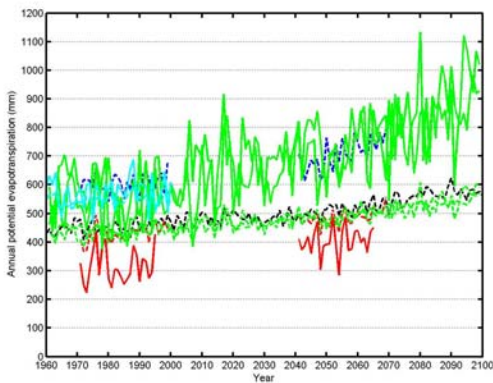
Bow at Calgary (Gauge 11)



N. Sask. (Gauge 12)



Marias (Gauge 13)



Battle (Gauges 17/18)

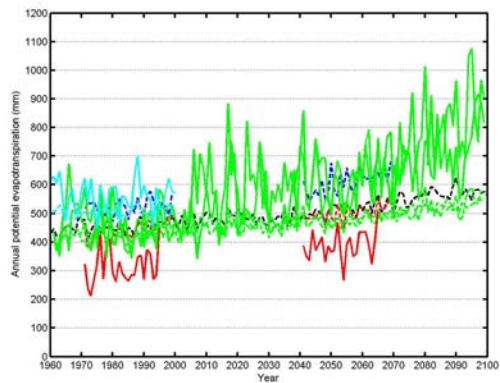


Figure 19: Time series of annual total potential evapotranspiration (mm), 1960-2100. Solid lines indicate PET calculated using the simplified Penman method; dashed lines indicate the Thornthwaite method. Observed – cyan; CGCM3 T47 – black; CRCM – green; RCM3 – red; HRM3 – blue.

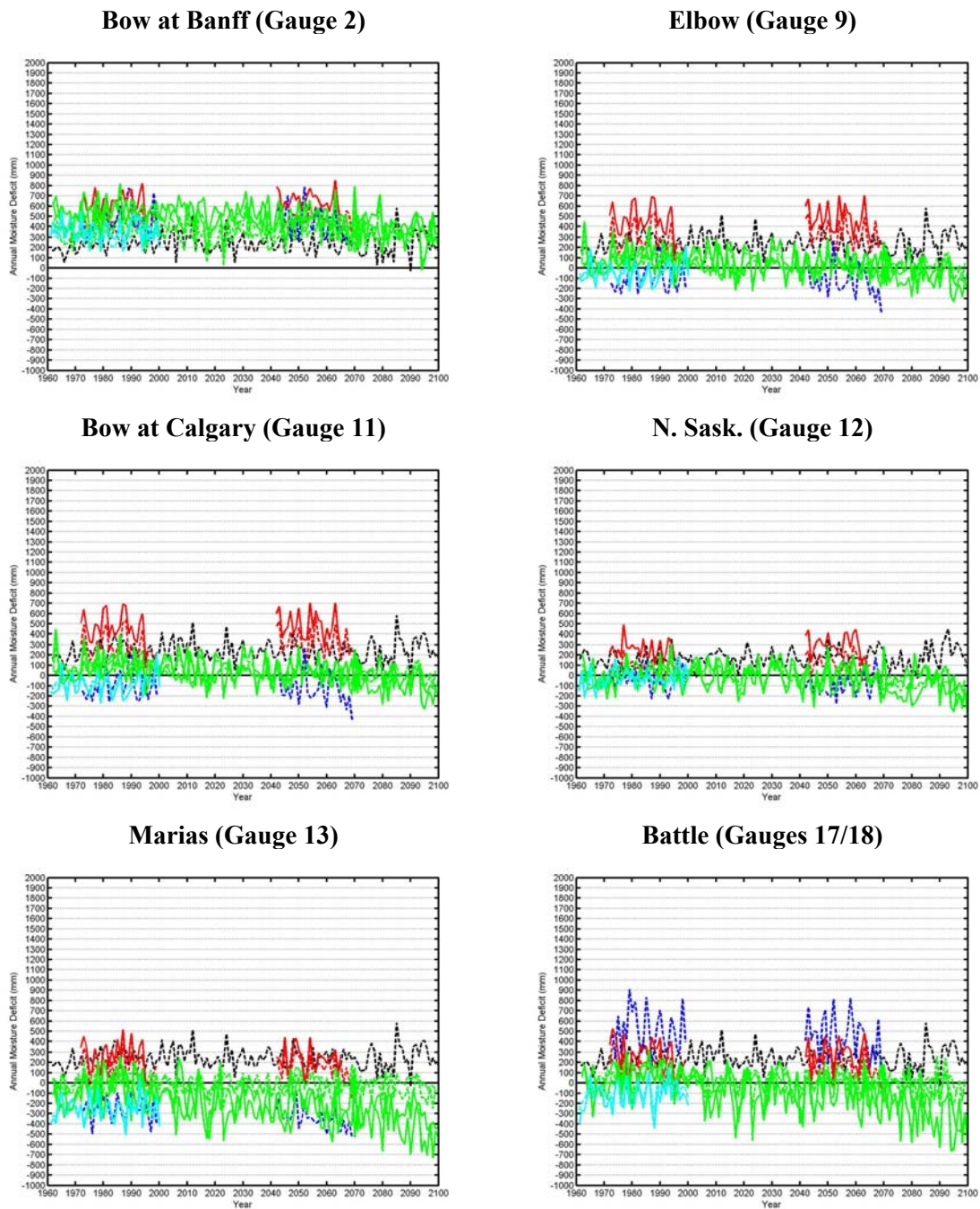


Figure 20: Time series of annual total moisture deficit (mm), 1960-2100, for the water year (October – September). Solid lines indicate PET calculated using the simplified Penman method; dashed lines indicate the Thornthwaite method. Observed – cyan; CGCM3 T47 – black; CRCM – green; RCM3 – red; HRM3 – blue.

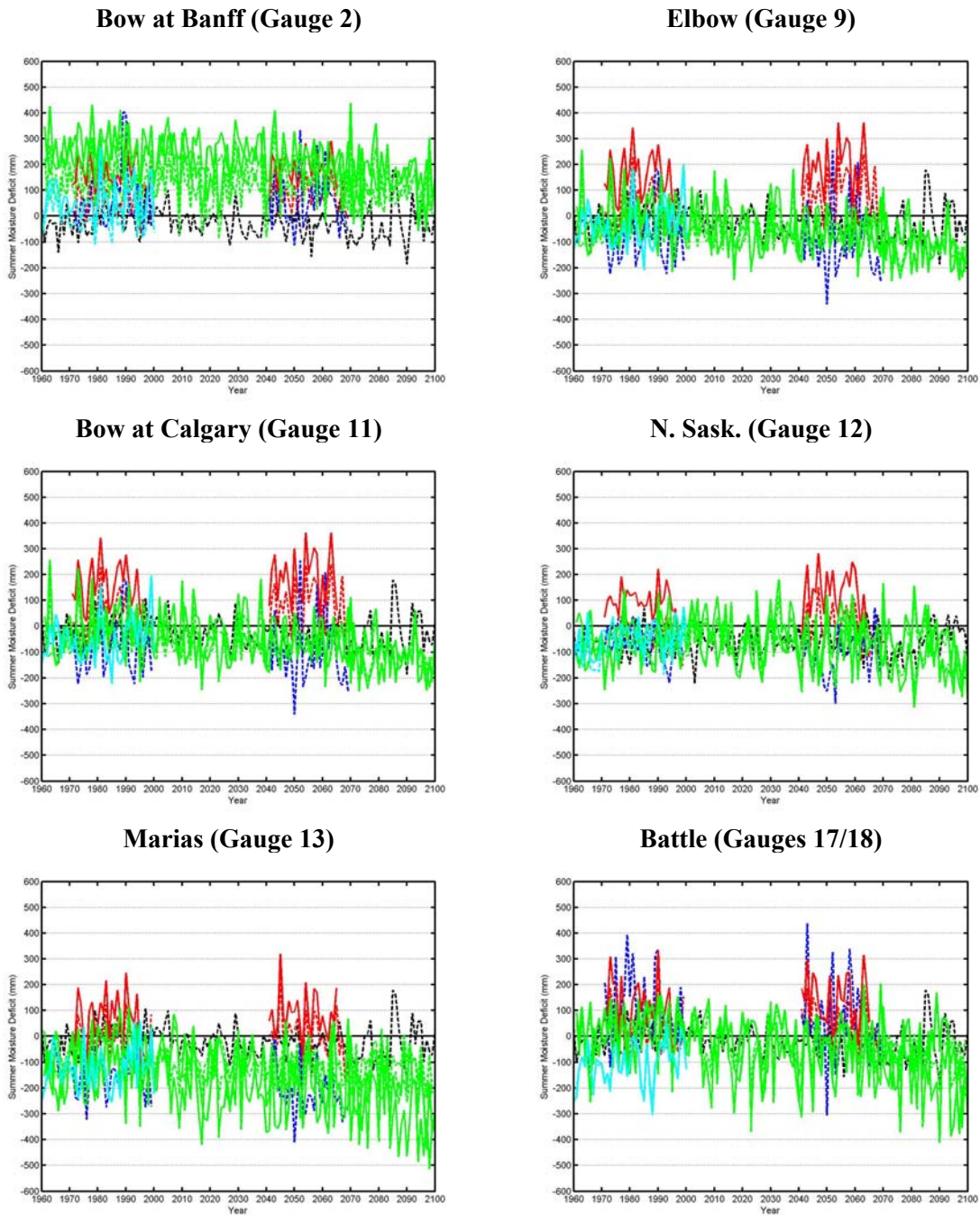
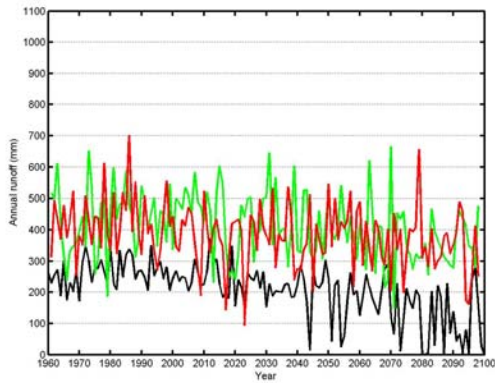
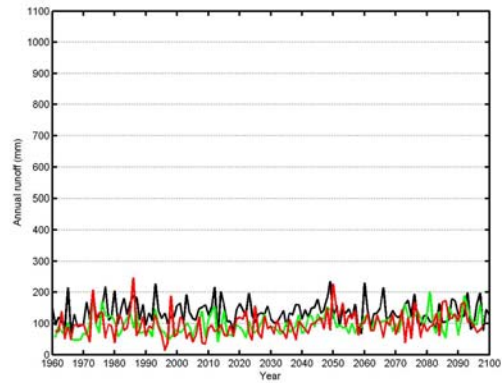


Figure 21: Time series of summer (May-June-July) total moisture deficit (mm), 1960-2100. Solid lines indicate PET calculated using the simplified Penman method; dashed lines indicate the Thornthwaite method. Observed – cyan; CGCM3 T47 – black; CRCM – green; RCM3 – red; HRM3 – blue.

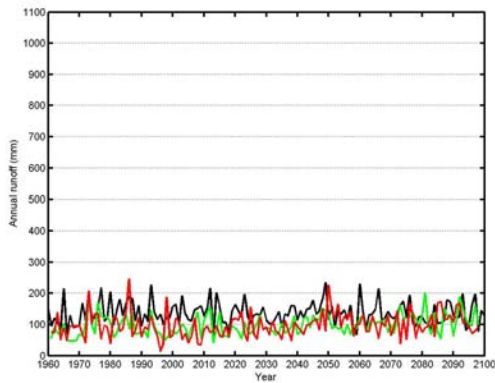
Bow at Banff (Gauge 2)



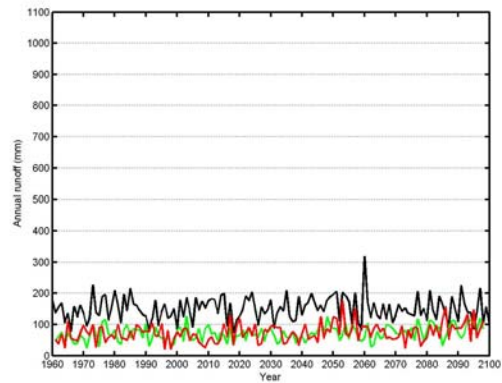
Elbow (Gauge 9)



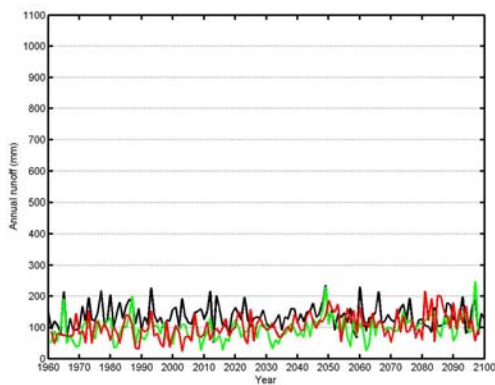
Bow at Calgary (Gauge 11)



N. Sask. (Gauge 12)



Marias (Gauge 13)



Battle (Gauges 17/18)

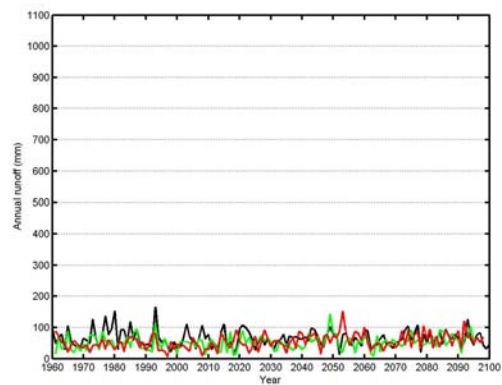


Figure 22: Time series of annual total runoff (mm), 1960-2100. CGCM3 T47 – black; CRCM aet – green; CRCM aev – red.

Probabilistic Scenarios – where do we go from here?

Numerous climate models have now been run for common sets of experiments, producing large datasets of projections of future climate for various scenarios (Tebaldi and Knutti, 2007). Impacts and adaptation researchers are now faced with the dilemma of how many and which climate change scenarios to select for use in their studies. They are also often asked to provide some sort of indication of the uncertainty associated with these scenarios. The general advice is to use enough scenarios to span the range of future climate, as well as a median, or mid-range, scenario (IPCC-TGICA, 2007). This often means that the focus of these studies tends to be on the potential impacts of the extremes of possible future climate which, while providing valuable information, does not allow for the consideration of the relative likelihood of future impacts (Brekke *et al.*, 2008). By considering ensembles of climate projections, impacts may be communicated in terms of risk rather than isolated examples of possible impacts and relative- or consensus-based likelihoods of various scenarios can be estimated by fitting a climate projection density function to an ensemble of climate projections (Brekke *et al.*, 2008). These density functions generally only represent a limited portion of the climate change uncertainties and several methods have been proposed for generating such density functions (Tebaldi *et al.*, 2005; Dettinger, 2006).

Tebaldi and Knutti (2007) provide a good review of the evolution of probabilistic treatments of GCM output over the last ten years or so, starting with the relatively simple approach of Räisänen and Palmer (2001), who used 17 GCMs and calculated probabilities of threshold events (e.g., that the warming at the time of CO₂ doubling will be greater than 1°C) from the fraction of models that simulated such an event. Giorgi and Mearns (2002) introduced the reliability ensemble average (REA) approach (all models are *not* considered to be equal) to model performance in simulating current climate, and inter-model agreement in the projections of future change guided the weighting of the models used. More recently, Dettinger (2005, 2006) has used resampling techniques to generate sufficient scenarios (based on GCM output) to construct a smooth probability density function. GCMs involved in the resampling process can be weighted according to performance. Most recently, Murphy *et al.* (2009) have used results from perturbed physics ensembles (PPE) experiments (e.g., Frame *et al.*, 2009) to construct probability density functions for a large number of variables over the UK. Unlike other studies which have made use of available GCM output, Murphy *et al.* (2009) focussed on attempting to define the range of climate model uncertainty by performing hundreds of GCM experiments using different initial conditions, parameter values and model structures.

Unfortunately there is insufficient RCM data available over western Canada to allow the construction of probabilistic scenarios based solely on these high resolution simulations, i.e., the sample size is simply too small. However, RCM results can be used in conjunction with those from GCMs to provide an indication of where they lie on a probability density function constructed based on GCM results (see, for example, Figure 23). The simplest approach is to construct crude probability density functions using all available GCM output (see Table 4 for a current summary of available GCM experiments). Results from PPE experiments (such as those available from climateprediction.net) may also be utilised. A more complex approach would be to then weight models according to their performance, which can be done in a number of ways with consideration of performance at both regional and global scales (e.g., Giorgi and Mearns, 2002; Brekke *et al.*, 2008). Probability density functions can then be generated based simply on the GCM output considered, or by using resampling techniques (e.g., Dettinger, 2005, Leander and Buishand, T., 2006). The final result will allow the calculation of the probabilities of relevant hydroclimate events for present and future conditions.

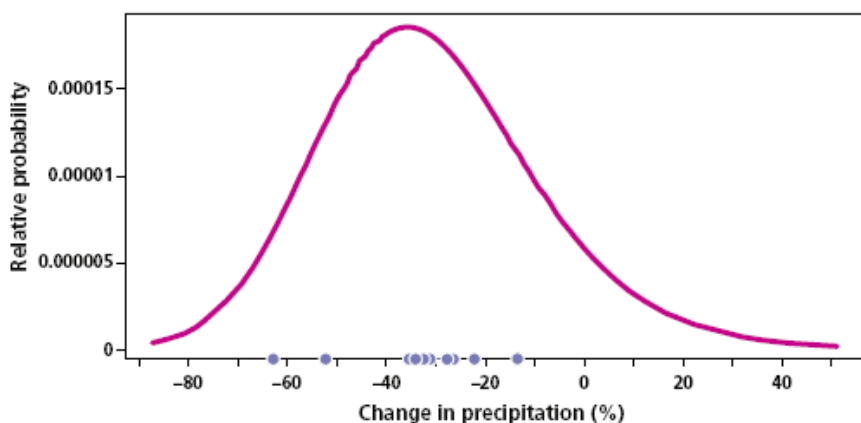


Figure 23: A probability distribution function of change in mean summer precipitation by the 2080s for a location in the UK. The added blue dots show the same change as projected by each of an 11 member RCM ensemble. [Source: Murphy *et al.* (2009)].

Table 4: Monthly mean atmosphere data availability from the Program for Climate Model Diagnosis and Intercomparison at Lawrence Livermore National Laboratory. Coloured cells indicate multiple experiments available.

	PICNTRL	20C3M	SRESA2	SRESA1B	SRESB1
*BCCR – BCM2.0, Norway	1	1	1	1	1
CGCM3.1 (T47) Canada	1	5	5	5	4
CGCM3.1 (T63) Canada	1	1		1	1
CNRM-CM3, France	1	1	1	1	1
*CSIRO-Mk3.0, Australia	2	3	1	1	1
CSIRO-Mk3.5, Australia	1	1	1	1	1
ECHAM4/MPI-OM, Germany	1	4	3	4	3
ECHO-G, Germany/Korea	1	5	3	3	3
FGOALS-g1.0, China	3	3		3	3
GFDL-CM2.0, USA	1	3	1	1	1
GFDL-CM2.1, USA	1	3	1	1	1
*GISS-AOM, USA	2	2		2	2
GISS-EH, USA	1	5		4	
GISS-ER, USA	1	9	1	5	1
INGV-SXG, Italy	1	1	1	1	
*INM-CM3.0, Russia	1	1	1	1	1
IPSL-CM3, France	1	2	1	1	1
*MIROC3.2 (hires), Japan	1	1		1	1
*MIROC3.2 (medres), Japan	1	3	3	3	3
MRI-CGCM2.3.2, Japan	1	5	5	5	5
NCAR-CCSM3, USA	2	9	5	7	8
NCAR-PCM, USA	1	4	4	4	4
UKMO-HadCM3, UK	2	2	1	1	1
UKMO-HadGEM1, UK	1	1	1	1	
*Models with maximum and minimum temperature available.					

Recommendations

The above analysis has shown that regional climate models do provide a more realistic picture of average climate over western Canada, particularly for precipitation. It is unfortunate that the limited sample size does not allow for their specific inclusion in a probabilistic analysis of future climate change, although their results can be placed in context with those from GCMs. The next stage of this work requires some consultation and decisions to be made about the complexity of any future analyses. The following are thoughts that need to be considered prior to continuing with the analysis.

1. Decide which hydroclimate variables are to be used in a probabilistic analysis. If these variables require calculation of potential evapotranspiration, then an appropriate methodology should be selected. Although the simplified Penman method seems to have more biogeographic meaning, the Thornthwaite method requires fewer climate variables and therefore will result in a larger ensemble of GCM results to be used in the construction of probability density functions. At the same time, particular threshold events which have meaning for the hydroclimate of western Canada should be identified. At this stage, a 'quick and dirty' probabilistic analysis can be undertaken based solely on the currently available GCM results.
2. Decide upon the approach for construction of probability density functions. The choice here is between perturbed physics experiments and resampling of available GCM output. Thousands of GCM results are available from PPE experiments from the climateprediction.net web site.
3. Process the relevant GCM data and construct derived hydroclimate variables, as necessary.
4. Decide whether or not the GCM data will be weighted in some manner to account for model performance. If yes, then decide upon a methodology to do this and on the level of complexity required.
5. Construct probability density functions on a grid box by grid box basis. Add RCM results to the pdfs to provide an indication of where the RCM results lie compared to those of the GCMs.

Acknowledgements

The following are thanked for their help in the preparation of this report: Christian Saad and Philippe Gachon of the University of McGill for help with mapping of RCM data; Dan McKenney and Pia Papadopol for supplying the gridded observed data derived using ANUSPLIN. RCM3 and HRM3 data were obtained from the NARCCAP web site and Seth McGinnis answered some questions concerning data formats. CRCM data were obtained from the Canadian Centre for Climate Modelling and Analysis.

References

- Brekke, L.D., Dettinger, M.D., Maurer, E.P. & Anderson, M. (2008): Significance of model credibility in estimating climate projection distributions for regional hydroclimatological risk assessments. *Climatic Change* **89**, 371-394.
- Dettinger, M.D. (2005): From climate-change spaghetti to climate-change distributions for 21st century California. *San Francisco Estuary and Watershed Science* **3**(1), 1-14.
- Dettinger, M.D. (2006): A component-resampling approach for estimating probability distributions from small forecast ensembles. *Climatic Change* **76**, 149-168.
- Flato, G.M. and G.J. Boer (2001): Warming Asymmetry in Climate Change Simulations. *Geophys. Res. Lett.* **28**, 195-198.

- Frame, D.J., Aina, T., Christensen, C.M., Faull, N.E., Knight, S.H.E., Piani, C., Rosier, S.M., Yamazaki, K., Yamazaki, Y. & Allen, M.R. (2009): The climateprediction.net BBC climate change experiment: design of the coupled model ensemble. *Philosophical Transactions of the Royal Society A* **367**, 855-870.
- Giorgi, F. & Mearns, L. (2002): Calculation of average, uncertainty range and reliability of regional climate changes from AOGCM simulations via the 'reliability ensemble averaging' (REA) method. *Journal of Climate* **15**, 1141-1158.
- Gordon C., Cooper, C., Senior, C.A., Banks, H.T., Gregory, J.M., Johns, T.C., Mitchell, J.F.B. & Wood, R.A. (2000): The simulation of SST, sea ice extents and ocean heat transports in a version of the Hadley Centre coupled model without flux adjustments. *Climate Dynamics* **16**, 147-168.
- Hogg, E.H. (1994): Climate and the southern limit of the western Canadian boreal forest. *Canadian Journal of Forest Research* **24**, 1835-1845.
- Hogg, E.H. (1997): Temporal scaling of moisture and forest-grassland boundary in western Canada. *Agricultural and Forest Meteorology* **84**, 115-122.
- IPCC-TGICA (2007): *General Guidelines on the Use of Scenario Data for Climate Impact and Adaptation Assessment*. Version 2. Prepared by T.R. Carter on behalf of the Intergovernmental Panel on Climate Change, Task Group on Data and Scenario Support for Impact and Climate Assessment, 66pp.
- Leander, R. & Buishand, T.A. (2007): Resampling of regional climate model output for the simulation of extreme river flows. *Journal of Hydrology* **332**, 487-496.
- Mantua, N.J., Hare, S.R., Zhang, Y., Wallace, J.M. & Francis, R.C. (1997): A Pacific interdecadal climate oscillation with impacts on salmon production. *Bull. Amer. Meteorol. Soc.* **78**, 1069-1079.
- Milewska, E.J., Hopkinson, R.F. & Niitsoo, A. (2005): Evaluation of geo-referenced grids of 1961-1990 Canadian temperature and precipitation normals. *Atmosphere-Ocean* **43**(1), 49-75.
- Murphy, J.M., Sexton, D.M.H., Jenkins, G.J., Boorman, P.M., Booth, B.B.B., Brown, C.C., Clark, R.T., Collins, M., Harris, G.R., Kendon, E.J., Betts, R.A., Brown, S.J., Howard, T.P., Humphrey, K.A., McCarthy, M.P., McDonald, R.E., Stephens, A., Wallace, C., Warren, R., Wilby, R., Wood, R.A. (2009): *UK Climate Projections Science Report: Climate change projections*. Met. Office Hadley Centre, Exeter, 191pp.
- Pope et al. 2000: The impact of new physical parameterizations in the Hadley Centre climate model: HadAM3. *Climate Dynamics* **16**, 123-146.
- Räisänen, J. & Palmer, T.N. (2001): A probability and decision-model analysis of a multimodel ensemble of climate change simulations. *Journal of Climate* **14**, 3212-3226.
- St. Jacques, J-M., Sauchyn, D.J. & Zhao, Y. (2010): Northern Rocky Mountain streamflow records: global warming trends, human impacts or natural variability? *Geophysical Research Letters* (in press).
- Shaw, E.M. (1994): *Hydrology in Practice*. 3rd Ed. Stanley Thornes (Publishers) Ltd., Cheltenham, UK, 569pp.
- Tebaldi, C., Smith, R., Nychka, D. & Mearns, L. (2005): Quantifying uncertainty in projections of regional climate change: a Bayesian approach to the analysis of multi-model ensembles. *Journal of Climate* **18**, 1524-1540.
- Tebaldi, C. & Knutti, R. (2007): The use of the multi-model ensemble in probabilistic climate projections. *Philosophical Transactions of the Royal Society A* **365**, 2053-2075.